UNIVERSITY OF CINCINNATI

April 17th , 20 07

I, Timothy G. S. Overly **,**
hereby submit this as part of the requirements for the degree of:

Master of Science

in:

Mechanical Engineering

It is entitled:

Development and Integration of Hardware and Software for Active-sensors in Structural Health Monitoring

Approved by:

Dr. Randall J. Allemang

Dr. Gyuhae Park

Dr. Mark Schulz

This page intentionally left blank.

Development and Integration of Hardware and Software for Active-sensors in Structural Health Monitoring

A thesis submitted to the Division of Research and Advanced Studies of the University of Cincinnati in partial fulfillment of the requirements for the Degree of

MASTER OF SCIENCE

From the Department of Mechanical, Industrial and Nuclear Engineering of the College of Engineering

2007

by

Timothy G. S. Overly

B.S.M.E., University of Cincinnati, 2002

Committee:

Chair: Dr. Randall J. Allemang
Dr. Gyuhae Park
Dr. Mark J. Schulz

Abstract

Structural Health Monitoring (SHM) promises to deliver great benefits to many industries. Primarily among them is a potential for large cost savings in maintenance of complex structures such as aircraft and civil infrastructure. However, several large obstacles remain before widespread use on structures can be accomplished. The development of three components would address many of these obstacles: a robust sensor validation procedure, a low-cost active-sensing hardware and an integrated software package for transition to field deployment. The research performed in this thesis directly addresses these three needs and facilitates the adoption of SHM on a larger scale, particularly in the realm of SHM based on piezoelectric (PZT) materials.

The first obstacle addressed in this thesis is the validation of the SHM sensor network. PZT materials are used for sensor/actuators because of their unique properties, but their functionality also needs to be validated for meaningful measurements to be recorded. To allow for a robust sensor validation algorithm, the effect of temperature change on sensor diagnostics and the effect of sensor failure on SHM measurements were classified. This classification allowed for the development of a sensor diagnostic algorithm that is temperature invariant and can indicate the amount and type of sensor failure.

Secondly, the absence of a suitable commercially-available active-sensing measurement node is addressed in this thesis. A node is a small compact measurement device used in a complete system. Many measurement nodes exist for conventional passive sensing, which does not actively excite the structure, but there are no measurement nodes available that both meet

the active-sensing requirements and are useable outside the laboratory. This thesis develops hardware that is low-power, active-sensing and field-deployable. This node uses the impedance method for SHM measurements, and can run the sensor diagnostic algorithm also developed here.

Finally, the need for an integrated system for SHM is of primary consideration in this thesis. Without such a system the widespread adoption of SHM will not take place, and this thesis addresses the issue by developing an integrated SHM solution. The solution incorporates active-sensing impedance-measurement based hardware and software with a combination of existing damage-detection algorithms. The result is an integrated system for in-field measurement, validation and analysis of structures. The system specifically incorporates the sensor validation procedure and sensor node also developed in this thesis. In conclusion, recommendations for the future direction of this research topic are made.

Acknowledgements

There are several people that I could not have completed my thesis without. Dr. Gyuhae Park is one, with kind words and positive encouragement he pushed me to finish this paper. I have never met someone so willing to edit a paper and give high quality advice on it. You are also knowledgeable and forward looking and I thank you for your advice. Without Chuck Farrar and the Engineering Institute, I would not have had a position in Los Alamos to come to.

Dr. Allemang was always available to me as an advisor and mentor, particularly during my graduate education and helped me obtain my first summer school position in Los Alamos, which allowed me to work on my thesis there, to my great benefit. I would also like to thank the other member of my committee, Dr. Mark Schulz, who, despite time constraints, was able to assist me.

I would like to thank those people who have shaped me. In particular I would like to thank my wife for following me to the little rainy town of Los Alamos, and allowing me to fulfill my requirements for this degree. My family is always a part of who I am and what I do; they are my mold.

Kassy, thank you for helping me take data, and doing some of the plotting necessary. Piero you were a great help as a partner with LaTeX, I doubt I would have gotten the nomenclature to work without your Google ability. Anthony thank you for your help with the Lamb wave dispersion curves. Matt, what can I say, it is MATlab.

Contents

List of Figures

List of Tables

Nomenclature

$\bar{\varepsilon}_{33}^{T}$	Complex Electric Permittivity
$\bar{T}$	Complex Tangent Ratio
$\bar{Y}^{E}$	Complex Young's Modulus
κ	Wave Number
θ_{reg}	Phase of Measurement
A_0	Asymmetric Mode
B_{reg}	Imaginary Register Value
d_{31}	Piezoelectric Coupling Constant
G_{reg}	Real Register Value
GF	Gain Factor
h	Height of PZT Transducer
l	Length of PZT Transducer
R_{cal}	Calibration Resistance
R_{imp}	Real Impedance
R_{out}	DC Chip Impedance
S_0	Symmetric Mode
w	Width of PZT Transducer
X_{imp}	Imaginary Impedance
$Y(\omega)$	Electromechanical Admittance
Y_{reg}	Magnitude of the Registers

Y_{reg} Register Magnitude

$Z_a(\omega)$ Mechanical Impedance of the PZT Transducer

$Z_s(\omega)$ Mechanical Impedance of Structure

$Z_{a,eff}(\omega)$ Effective Mechanical Impedance of the PZT Transducer

Z_{imp} Impedance Magnitude

Z_{reg} Magnitude of the Registers

$Z_{s,eff}(\omega)$ Effective Mechanical Impedance of Structure

Chapter 1

Introduction

1.1 Structural Health Monitoring

Structural Health Monitoring (SHM) is the process of continuously monitoring a structure for degradation or damage. This method is different from non-destructive evaluation (NDE) in that SHM is done in-situ on the structure and is done on a near-continuous basis. The sample rate that is required for continuous monitoring is different for every structure, and is application specific. SHM would lead to large cost savings by allowing for the migration from time-based to condition-based maintenance [1]. A definition for SHM that has been presented is that it will provide valid, reliable and accurate operational data upon which life-cycle management decisions can be made [2], meaning that the SHM system would provide enough information to allow for use of a structure for the maximum amount of time between required maintenance periods. There is also the potential for SHM systems to operate in two modes. In the first mode, the system could periodically check the structure for aging and degradation from use and age. The second mode, the system could rapidly assess the structure after an extreme event, such as an earthquake [3].

The two types of structures that would benefit most from SHM would be, firstly, structures that have large safety factors in the design for longevity of service, and secondly, systems where

their weight critical nature requires routine inspections. These two types of structures comprise most of the engineering systems in the world. With the addition of a SHM system, the over designed systems could be redesigned to save on material costs, and required inspections on the weight critical systems could be substantially reduced [1].

An example of an area that might be considered a subset of SHM is the condition monitoring (CM) of rotating machinery, and according to Farrar and Worden [4], CM is the most successful type of SHM to be employed to date. However, many challenges for the broader SHM field still remain. Farrar and Worden outline some of the largest challenges to the current state of SHM. The prime challenge is ability to detect damage, which manifests itself as local changes, using global responses of the structure. This problem arises because of the limited number of sensors in any given SHM system, and the inability to monitor every aspect of the system. A second major obstacle is that signals from damaged structures are not usually available, and the time-scales involved make it hard to achieve accurate repeatable measurements. The third challenge is to develop an idea of what capability is needed from the sensor network before it is placed in the field. This capability would be determined by type of measurement to be made and the level of redundancy required in its measurement ability. The redundancy would include the ability to validate the sensor network. As with CM, general SHM will require time and effort to produce the proper hardware and software for reliable monitoring in real world settings.

1.2 Piezoelectric Active Monitoring for SHM

Structural Health Monitoring is a field that has received quite a bit of attention from the engineering research community in recent years, and in particular, SHM measurements that are based on active materials for sensing. One very prominent type of active materials are piezoelectric materials. Piezoelectric materials fall into the “smart” materials field. Smart materials

transform one type of energy into another type. A piezoelectric material transforms mechanical energy, in the form of stress, into electrical energy (direct effect), or conversely, electrical energy into mechanical energy in the form of strain (converse effect). These two effects are demonstrated graphically in Figure 1.1. The direct and indirect effects can be used to sense and actuate a structure respectively. As sensors, piezoelectric materials are found readily in accelerometers. As actuators they can be used to both send signals and mechanically influence the structure. They are inexpensive, fairly robust and can be highly customized in shape and size.

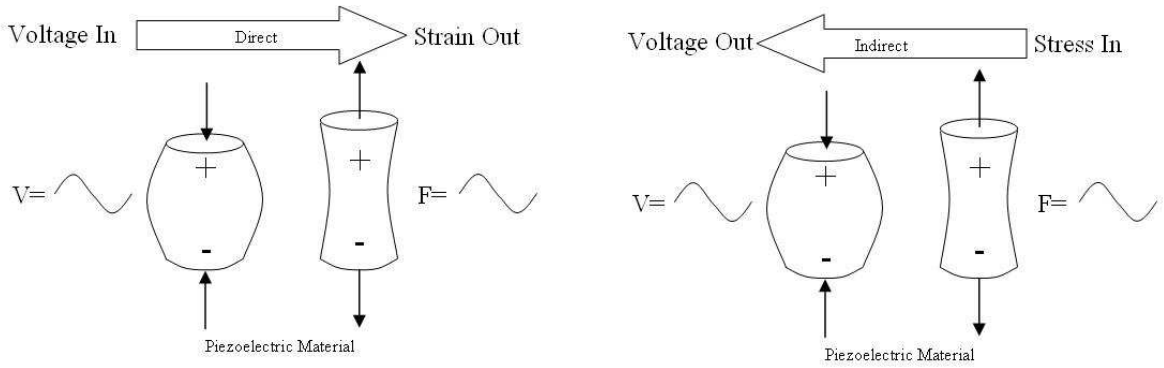

(a) Direct (b) Indirect

Figure 1.1: Two different operating modes of piezoelectric materials

Piezoelectric materials they have been used as sensor/actuators for many years because of their unique characteristics. There are two main types of sensing/actuations that are done with piezoelectric materials in the SHM field.

The first technique is the impedance method. The impedance method is made possible by the coupling that occurs when a PZT patch is bonded to a structure. The electrical impedance of the patch and the mechanical impedance of the structure become coupled and by measuring the electrical impedance, the mechanical impedance can be obtained, and therefore the state of the structure can be deduced.

The second technique that will be discussed is the Lamb wave propagation technique,

which uses PZT transducers in a pitch-catch (one sensor sends a signal and another receives the signal) or pulse-echo (same sensor sends and receives the signal) configuration. This technique uses previously recorded baseline readings and signal processing to determine whether the structure in between the sensors or in the area of the sensors has changed.

1.2.1 Impedance-based Structural Health Monitoring

Liang et al. [5] was the first to develop the theory for impedance based measurements for use in SHM. The theory has been substantially developed by Park et al. [6, 7, 8], Bhalla et al. [9, 10], Giurgiutiu et al. [11, 12, 13] and Sun et al. [14].

The basic concept of the impedance method is to use high frequency vibrations to monitor the local area of a structure for changes in structural impedance that would indicate damage or structural change. The monitoring is made possible by using piezoelectric (PZT) sensor/actuators whose electrical impedance is directly related to the structure's mechanical impedance. The impedance measurements can easily give information on changing parameters, such as resonant frequencies or damping, which allows for the detection and location of damage.

The expression for one dimensional electromechanical admittance ($Y(\omega)$), that was developed by Liang et al., is given in Equation 1.1.

$$Y(\omega) = \omega i \frac{wl}{h}\left(\bar{\varepsilon}_{33}^{T}(1-i\delta) - d_{31}^{2}\bar{Y}^{E} + \frac{Z_a(\omega)}{Z_s(\omega)+Z_a(\omega)} d_{31}^{2}\bar{Y}^{E}\left(\frac{\tan\kappa l}{\kappa l}\right)\right) \tag{1.1}$$

Where w, l, and h are width, length and height of the PZT patch respectively. $Z_s(\omega)$ and $Z_a(\omega)$ are the mechanical impedances of the host structure and of the PZT transducer respectively, κ is the wave number, $\bar{Y}^E$ is the complex Young's modulus, and $\bar{\varepsilon}_{33}^{T}$ is the complex electric permittivity of the PZT transducer. In addition $Z_a(\omega)$ is also defined by Equation 1.2.

$$Z_a(\omega) = \frac{\kappa w h \bar{Y}^E}{i\omega \tan \kappa l} \tag{1.2}$$

And finally for the one dimensional case, the wave number is defined in Equation 1.3.

$$\kappa = \omega \sqrt{\frac{\rho}{\bar{Y}^E}} \tag{1.3}$$

The previous formulas were further expanded by Bhalla and Soh [10], who solved the two dimensional governing equation for $Y(\omega)$, which is given in Equation 1.4.

$$Y(\omega) = \omega i \frac{l^2}{h} \left(\bar{\varepsilon}_{33}^T - \frac{2 d_{31}^2 \bar{Y}^E}{(1-\nu)} + \frac{2 d_{31}^2 \bar{Y}^E}{(1-\nu)} \left(\frac{Z_{a,eff}(\omega)}{Z_{s,eff}(\omega) + Z_{a,eff}(\omega)} \right) \bar{T} \right) \tag{1.4}$$

Where $\bar{T}$ is the complex tangent ratio, which in an ideal situation would be equal to $\frac{\tan \kappa l}{\kappa l}$. Equation 1.4 introduces the idea of effective impedance, in $Z_{s,eff}(\omega)$ and $Z_{a,eff}(\omega)$. It can be seen how these two terms combine to couple the impedances of the structure and the piezoelectric patch. This coupling allows one to measure the mechanical impedance of the structure through the electrical impedance of the piezoelectric patch.

Once a PZT transducer has been bonded to the structure, the impedance-based SHM is able to monitor the high frequency region of the structure for local damage. The higher frequency range is more sensitive to local damage, as opposed to lower frequency which is more sensitive to global changes or operational condition changes in the system. It has been shown that the wavelength of the signal, used to detect damage of a given size, needs to be smaller than the characteristic length of the damage [15]. To satisfy this requirement and to be able to detect incipient damage, the frequency range of 30-400 kHz is usually used [8]. In addition, the maximum frequency considered should be below 500 kHz [16], above this frequency the sensing region is very small and is sensitive to the piezoelectric patch and its bonding conditions and not of the structure. However, depending on the measurement situation, the maximum

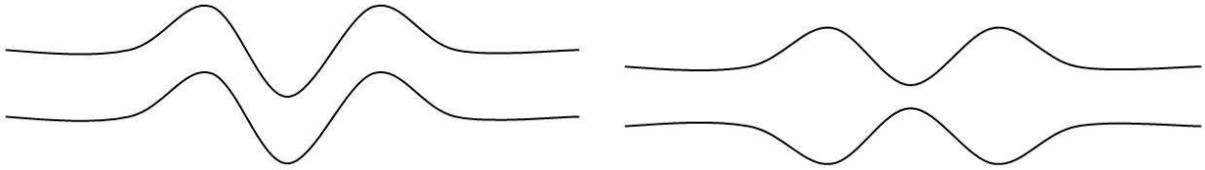

(a) Asymmetric Mode (A_0) (b) Symmetric Mode (S_0)

Figure 1.2: Diagrams of the two types of Lamb waves

frequency may be below this boundary.

There has been extensive research performed in recent years on the application of impedance measurements in the field of structural health monitoring. A good review on the topic is presented by Park et al. [8]. An important aspect of the impedance method is that the method requires significantly lower power compared to other active-sensing technologies, such as Lamb wave propagation. In addition to the lower power requirements, impedance measurements also have the potential to perform in-situ active sensor diagnosis [10, 6, 17] and is investigated further in Chapter 4.

1.2.2 Lamb Wave Propagations

Lamb wave propagation is another method that utilizes smart piezoelectric patches for damage detection. Wave propagation is the effect of a sharply applied localized disturbance on a medium, and how that effect is transmitted or spread throughout that medium [18]. The theory for the waves in an elastic infinite plate was originally presented by Horace Lamb [19] in 1916. Lamb waves consist of an infinite number of discrete modes that can be generated in the elastic medium. These waves can be categorized into two separate groups: Symmetric and Asymmetric. Symmetric modes are propagated in a compression wave fashion; they are mirrored about the centerline of the cross-section of the plate. Asymmetric modes are best described as transverse waves that travel along the plate [20]. A diagram of the two types of modes is shown in Figure 1.2.

The diagram shows the first fundamental mode of each of the types of waves. Each type would have an infinite number of possible mode shapes and correspondingly, an infinite number of mode numbers. Lamb waves in practice are a combination of the two types. In S_0 modes the particles in the medium are displaced in a direction parallel to the surface, and in A_0 modes the particles move in a normal direction to the surface.

In any material the various Lamb waves propagate at different velocities, they disperse. The velocity of a set of waves (group velocity) is a function of thickness of the medium and frequency of the wave. These dispersion curves come from solving the period equation, given in Equation 1.5 for symmetric modes and Equation 1.6 for asymmetric modes.

$$\frac{\tan qh}{\tan ph} = -\frac{4k^2pq}{(q^2-k^2)^2} \tag{1.5}$$

$$\frac{\tan qh}{\tan ph} = -\frac{(q^2-k^2)^2}{4k^2pq} \tag{1.6}$$

An example of a solution to the group velocity equations is shown in Figure 1.3(a), while another measurement of wave velocity, phase velocity is shown in Figure 1.3(b). These dispersions curves were generated for a 1.59mm thick aluminum plate. Dispersion curves are often shown in terms of $Frequency * Thickness$. This method of presentation is done to allow for the application of the curves to any thickness of plate, as long as the material remains constant.

The use of dispersion curves is a key requirement in the SHM field. It shows the relative speed at which different waves travel in a given material. These speeds are used to choose regions of excitation that is conducive to monitoring. These regions are chosen to have relatively few modes arrive at the sensing region at a given time. Separating the arrival times of the different waves facilitates the detection of changes in the signal, and thereby assists with damage detection.

Lamb waves for damage detection is not a new concept; it dates back at least fifty years

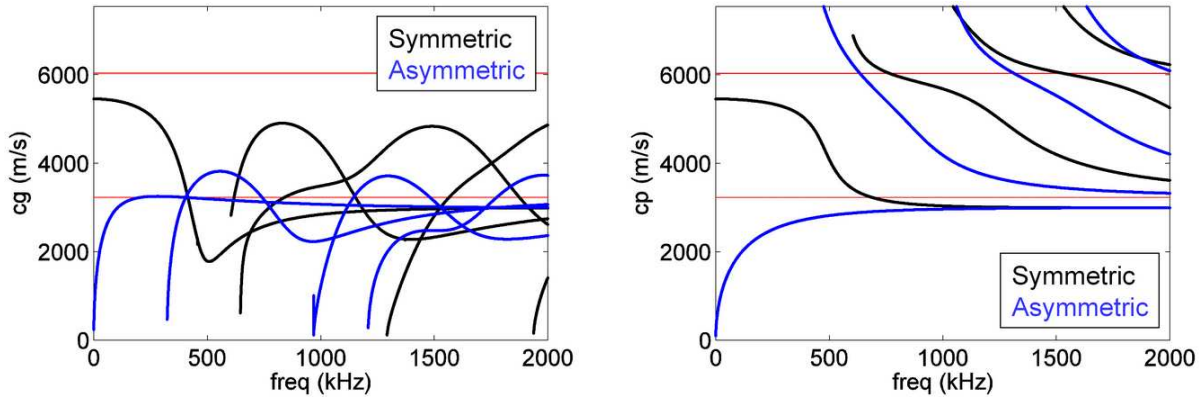

(a) Group Velocity (b) Phase Velocity

Figure 1.3: Examples of group velocity and phase velocity dispersion curves for a 1.6mm thick aluminum plate

[21]. Lamb wave and guided waves have been used to inspect a wide variety of structures. Dalton et al. [22] explored the potential of guided waves in aircraft fuselages. Rose et al. [20] have investigated the potential for guided waves to detect damage in railroads. Defects in pipes were examined by Lowe et al. [23], and Cawley and Alleyne [24] discussed the use of Lamb waves for monitoring large structures.

There are two main methods that are employed with Lamb wave propagations. The two methods are pitch-catch and pulse-echo. The first, pitch-catch, is very similar to pitcher and catcher in baseball. One sensor/actuator throws the "ball", a specific signal of chosen frequency content, and another sensor/actuator catches the "ball" and records it. This technique allows for comparison to baseline measurements, and for various signal processing to determine if some damage or change has occurred along the signal path. The second method is "pulse-echo", and is where one sensor/actuator sends a signal out and then listens for reflection signals. In the same way as pitch-catch, the recorded signal can be compared to previously recorded baselines and used to determine changes in the system.

Sensor failure can also cause the Lamb wave signal to change, which might be interpreted as damage to the system, even when no damage may have occurred. The effects of sensor

failure on Lamb wave measurements are examined in this thesis to classify the errors that may be introduced through sensor failure. The effects of sensor failure on Lamb wave measurement and impedance measurements are discussed in Chapter 2.

1.3 Active SHM Devices

There has been a push in recent years to develop active sensor nodes for use in SHM. Lynch and Loh [25] have produced a review of wireless sensor nodes that have been developed, with a section on active sensor nodes. The majority of the active sensor nodes, reviewed by Lynch and Loh, provide open ended active sensing capabilities, allowing for a variety of techniques and sensors to be used.

There are several drawbacks to the currently available active sensor nodes that will be addressed in this thesis. The first limitation among most of the active sensing nodes is that they do not have the necessary sampling frequency to perform SHM monitoring measurements greater than 50 kHz. This frequency range limits the types of structures that are able to be monitored with the devices. The second limitation is many of the devices have large power requirements that limit their ability to be deployed in real world situations. Because of the long term nature of SHM, conventional battery power for several months may not be sufficient. The ability for the device to be operational for long periods of time, years or even decades, is a prime consideration. The third limitation for many active systems is their current stage of development does not allow for field deployment. Two systems that were similar to the device that is developed in this thesis from Grisso [26] and Mascareñas [27] consisted of prototype evaluation boards, which are not environmentally durable and require more power than integrated solutions.

To the author's knowledge, there is no field deployable active SHM system available in an academic or commercial setting that allows for long term low power deployment. A goal for this thesis is the development of a device to meet the needs for a useable wireless impedance

device. The system that was preliminarily developed by Mascareñas [27] was used as a starting point for the integrated solution presented in Chapter 5.

1.4 Sensor Validation

Friswell and Inman [28] noted that sensor validation has received comparatively little consideration from the smart structures community. Sensor validation means the confirmation of functioning sensors during operation. Friswell and Inman [28] then proposed a technique for sensor validation by comparing the subspace of the response to the subspace of the lower modes of the structure, and allowed for the excess information available from the sensor network to be used for diagnosis. This technique was further developed by Abdelghani and Friswell [29]. They use new residual generation and evaluation techniques that allow for the detection of multiplicative and additive faults. Worden [30] used auto-associative neural networks and principal component analysis (PCA) to identify errant sensors used to measure correlated signals. These multi-sensor techniques use correlated data that will probably not be available in an impedance based SHM system; they also have a difficulty discriminating between sensor failure and structural damage.

Methods for specifically determining the health of piezoelectric patches have also been examined in previous research. A couple of the techniques specifically make use of the impedance measurements of the piezoelectric patch, although in different ways. Saint-Pierre et al. [31] uses the shape of the first real impedance resonance and its change to determine the state of the bonding condition. Guirgiutiu and Zagrai [13] propose a similar technique using the attenuation of the first imaginary impedance resonance for damage detection. Pacou et al. [32] discusses the use of the shift of the first natural frequency of the piezoelectric patch before and after bonding as a possible method for determining bonding condition.

There are several disadvantages to the above piezoelectric specific methods. First, they

are not sensitive to small debonding in the PZT transducer and sensor fracture could cause the resonance to move beyond the monitoring region. Second, they all require relatively high frequency measurements to determine the bonded first natural frequency. A standard impedance analyzer can be used to make a measurement into the 600 kHz range and up, which is needed in these methods. Current SHM nodes that are used for the impedance based SHM are not able to make impedance measurements into that range [25]. This frequency requirement makes these techniques generally unsuitable for field deployment using currently available sensor nodes. Finally the absolute number of data points that need to be collected for sensor diagnosis is quite high compared to the method proposed in this paper. The higher number of data points demands more from the SHM node, which generally have very limited storage capacity and RAM.

Bhalla and Soh [10], in addition to the formulations in Section 1.2.1 suggest that the imaginary part of the admittance measurement is more sensitive to bonding conditions, and therefore could be useful in determining the bond health. This relationship was further demonstrated by Park et al. [17, 6], who showed the initial relationship between bonding condition and the slope of the imaginary admittance measurement (susceptance). This technique is based on the admittance measurement of a free PZT transducer, which is shown in Equation 1.7 and the equation for the bonding layer's effect on the electrical admittance, which is given in Equation 1.8.

The equation for a PZT transducer in a free state that was developed in Park et al. [6] is given in Equation 1.7.

$$Y_{free}(\omega) = i\omega\frac{wl}{t_c}(\varepsilon_{33}^{T}(1 - i\delta)) \tag{1.7}$$

The equation for the bonding layer effects is achieved by allowing $Z_s(\omega)$ in Equation 1.1 approach infinity.

$$Y_{bond}(\omega) = i\omega\frac{wl}{t_c}(\varepsilon_{33}^{T}(1-i\delta) - d_{31}^{2}\bar{Y}_{p}^{E}) \tag{1.8}$$

Equations 1.7 and 1.8 show that the same PZT transducer will have a different admittance measurement by changing from a free-free condition to a surface-bonded condition. The bonding of the sensor would cause a downward shift in the electrical admittance of the free PZT transducer by a factor of $d_{31}^{2}\bar{Y}_{p}^{E}$. This change in slope would allow for the health of the bonding condition to be assessed with a measurement of the susceptance [6]. The assumption that $Z_s(\omega) = \infty$ is used because the stiffness and mass of the host structures is usually several orders of magnitude greater than that of the PZT transducer. This assumption allows for the signals of PZT transducers to be compared even on heterogeneous materials. Another assumption that is made, is the shear lag ratio, $\xi = \frac{S_p}{S_b} - 1$, is equal to 0 in a perfect bonding case. Several people including Crawley and de Luis [33], Sirohi and Chopra [34] and Park et al. [35] have investigated the shear lag effect on the strain transfer mechanisms on surface bonded PZT transducers. The effects of temperature on the susceptance signal will be investigated in order to design a robust sensor diagnostic algorithm. This investigation and classification procedure of susceptance signals is further reviewed in Chapter 2.

1.5 Integration of SHM Tools

To the author's knowledge there is no integrated solution for long-term low-power SHM. The measurement nodes available, generally do not meet the needs of the SHM community. If the hardware does have the necessary capabilities, it is generally not available for use in the field because of its prototype construction. Software for specialized SHM applications does exist in the form of individual data analysis programs and scripts. These programs perform data analysis on collected data and do not have the ability to control hardware for the purposes of making

measurements. A system was developed by Allen [3] that was an integration of hardware and software that could be used for SHM purposes, but the system required substantial continuous power at the measurement node. The main goal of this thesis is to make a step forward on integrating low-power hardware with flexible structural health monitoring software.

A structural health monitoring program that was originally developed at Los Alamos National Laboratory by Swartz et al. [36] can be used to monitor the health of plate structures (HOPS). HOPS has been improved since its original implementation and it currently has the ability to import and analyze both impedance and Lamb wave SHM information, and has been evolving over time into a integrated SHM environment. HOPS can currently control laboratory based hardware to make Lamb wave measurements. However this program lacks the ability to perform a couple key tasks required of an integrated environment. The first is its inability to control a field deployable SHM device and the second is its lack of meaningful sensor diagnostic algorithms. The integration of the statistical tools already found in HOPS with sensor diagnostic procedure and the sensor node also developed for this thesis would be a significant step forward to making an SHM system that is flexible and field deployable. The integrated solution is detailed in Chapter 6.

1.6 Contributions

The overall goal of this thesis is to improve the usability and make the field application of impedance based monitoring more universally obtainable. This goal was accomplished by creating an integrated package of hardware and software capable of making and analyzing structural health monitoring measurements based on the impedance method.

The contributions of the research and development that is summarized herein are:

- Investigation of various piezoelectric (PZT) failure modes and the effect these failures have on structural health monitoring (SHM) measurements.

- Research the effects of temperature on SHM measurements from PZT sensors.
- Development of a sensor diagnostic algorithm to automatically assess the health of piezoelectric sensors in the presence of temperature changes.
- Development of a unique compact wireless impedance measurement node for use in SHM and sensor diagnostics
- Development of an integrated package of low-power hardware and integrated software for use in SHM applications

1.7 Thesis Overview

This research and development is broken down into four main areas that are considered unique stages in the process.

The first part is to categorize various failure modes of PZT sensors and how those modes effect SHM measurements. Sensor failure categorization is further researched in Chapter 2, where various sensor failure modes and environmental effects on impedance measurements are examined.

The second task is to utilize the categorized sensor failure and environmental information and create a simple sensor diagnostic algorithm that can be used to determine sensor health. Chapter 4 shows the actual development of a procedure for sensor diagnostics.

The third aspect is to develop a field deployable sensor node capable of implementing the sensor diagnostic algorithm and making impedance based measurements. The hardware was designed to fill a niche of specialized measurement capabilities, low power and wireless data transmission. This hardware development is explained in detail in Chapter 5.

The final part of the thesis is to integrate the sensor diagnostic tools, wireless sensor node and a currently available SHM program to create a packaged solution that could be used in the

field to record and analyze data. The integration process is explained in Chapter 6.

Chapter 2

Sensor Failure and Temperature Effects on Impedance Measurements

2.1 Introduction

The structures being monitored by PZT transducers are usually subjected to various external loading and environmental conditions. These conditions may adversely affect the functionality of the SHM system. This effect is the reason an active sensor diagnostic process is a critical component to any robust SHM system. Due to the brittle piezoelectric ceramic materials, the fracture and degradation of the electromechanical properties are some of the most common types of sensor failure. Also of concern is the health of the bonding condition between the PZT transducer and the host structure. It is of concern because the bonding layer is a critical component in the coupling between the PZT transducer and the host structure which makes SHM possible.

A complete failure in a PZT transducer would, in general, be easily identifiable because of the complete loss of signal or from the reception of a totally unreasonable result. However, if the sensor is not completely failed, if the fracture or debonding is minor, then the measurement signal may be interpreted as structural damage. This situation would lead to a false positive, which would degrade the cost saving aspect that is a cornerstone of SHM. To the author's best

knowledge, the long-term reliability of the PZT transducers, the effects of sensor degradation and the features of sensor failure have not been sufficiently addressed.

As reviewed in greater detail in Section 1.4, it has been observed by several people including Park [6, 17] and Bhalla [10] that the imaginary admittance of the impedance measurement is an indication of bonding condition. As the piezoelectric patch is bonded to the structure the mechanical impedance of the structure and the electrical impedance of the patch become coupled. The slope of the susceptance signal from the PZT transducer is a measure of the capacitance. Park [6] indicated that an increase in slope corresponded to decrease in bonding percentage and a decrease in slope corresponded to possible breakage of the sensor. What was not done was to investigate the effects of environmental variance on the susceptance measurements or to systematically classify the effects of various PZT sensor failure modes. These investigations will allow for the development of a robust sensor diagnostic algorithm, and are performed in this chapter.

2.2 Feature Classification of Sensor Failure Modes

Since various types of sensor failure will affect the susceptance in different ways, the first step in the diagnostic process is to quantify those changes for different bonding conditions and sensor health. This classification will allow the susceptance to be used in a meaningful way in a sensor diagnostic procedure. The two main features of susceptance that are being examined are the slope and the standard deviation of the signal from that slope.

2.2.1 Patch Breakage

The first sensor failure mode to be investigated is sensor breakage. After a potentially damaging event on structure, it is possible that the PZT patch that is being used to monitor the structure may have been damaged, causing a potentially erroneous measurement of the struc-

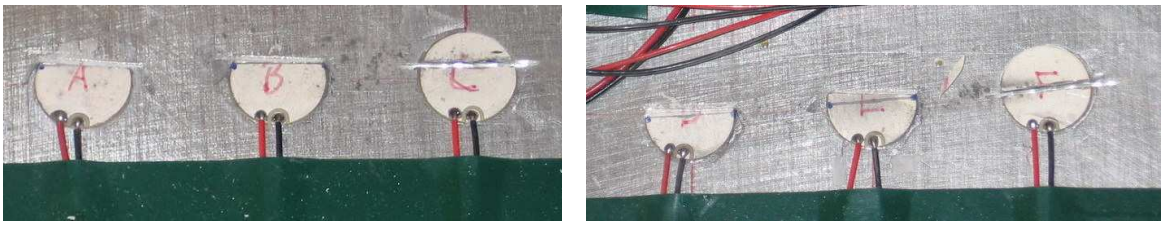

(a) 25 Percent (b) 50 Percent

Figure 2.1: The PZT patches were broken using both a chisel and an abrasive cutting wheel

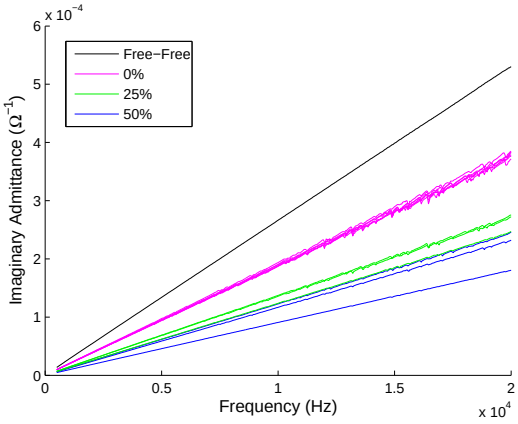

Figure 2.2: The slope of the imaginary admittance decreases as breakage area increases

ture. To investigate the effects of such an occurrence, six 12.7mm PZT patches were bonded to a 6.35mm thick aluminum plate and were broken or cut at specific percentages of their total area. After the damage was introduced, impedance measurements were taken. Three patches were broken or cut to reduce the total area by 25 percent, and three different patches were broken or cut at to reduce the total area by 50 percent. Two of each three were broken with a chisel, to more accurately simulate a damage event. The remaining patches were cut with an abrasive wheel to insure a more accurate reference case. Figure 2.1(a) shows the 25 percent breakage case, and Figure 2.1(b) shows the 50 percent breakage case.

Impedance measurement of these patches was taken prior to breakage and post breakage, allowing for a comparison of the actual change of capacitive value for each sensor. Imaginary

admittance measurements were taken of free-free baseline cases, and all the measurements are shown in Figure 2.2. It can be seen in Figure 2.2 that the slope of the imaginary admittance is proportional to the breakage percentage. As the percent increases, the slope decreases. The 25 and 50 percent broken sensors had a 20 and 33 percent reduction in susceptance slope respectively. There is some variance in the slopes of each group, which can most likely be attributed to the inconsistent nature of the fractures. Figure 2.1 shows that the post breakage patch fragments are not a consistent size, they are approximately a 25 and 50 percent reduction, but do have some variance. The line with the greatest decrease in slope corresponds to the cut 50 percent patch, which has the smallest final area, demonstrating a further correlation between final patch size and slope.

2.2.2 Debonding

Sensor debonding is a failure mode of considerable concern. It is of concern because unlike some of the other failure modes, it is not readily noticeable upon visual inspection. Debonding may occur in a situation where the structure may not have sustained any damage, i.e. a strain large for the PZT sensor but within the operating parameters of the structure or the long-term degradation of the adhesive bond.

To test the effects of debonding, sixteen 12.7mm PZT patches were bonded to a 6.35mm thick aluminum plate. Nine were bonded with epoxy and nine with super glue. In each set of nine, three were bonded fully, three were bonded with 25 percent debonding and the remaining three were bonded at 50 percent. Two adhesives were used to test if different adhesives contribute differently to the change in susceptance. This simulation of debonding was achieved by using release paper to restrict the bonding percentages of the sensor. Specifically, the PZT patch was bonded a corresponding percent of the total area on top of double layer of release paper. Photos of the bonded sensors are shown in Figure 2.3.

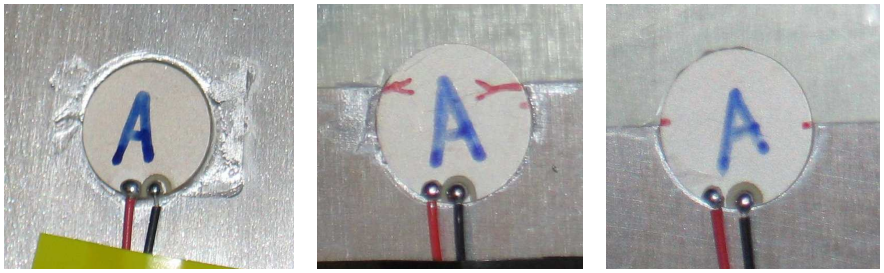

(a) 0% Debonding (b) 25% Debonding (c) 50% Debonding

Figure 2.3: Various debonding percentages on 12.7mm PZT patches

The debonding of the sensors has an effect on the sensor diagnostic indicator that is being examined, the slope of the susceptance. The slope changes in a repeatable and consistent manner with debonding percentages. Figure 2.4 shows two graphs, both at room temperature, of the effect of debonding percentages on the susceptance. Figures 2.4(a) and 2.4(b) are of super glue and epoxy bonded patches respectively. The slope of the susceptance decreases with debonding. It can be seen in each graph that there is a progression of the measurements from the highest slope, a reference free-free set, to the lowest slope, the fully bonded case. This decrease is consistent with a previous study [6], but this investigation shows that the percent of change not only indicates debonding, but also the amount of debonding.

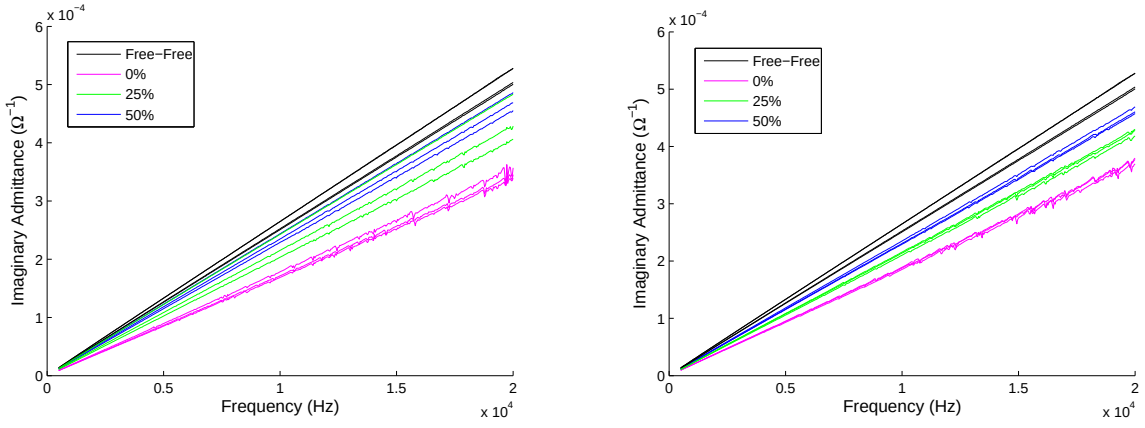

(a) Super Glue (b) Epoxy

Figure 2.4: The slope of the susceptance increases with debonding percentage

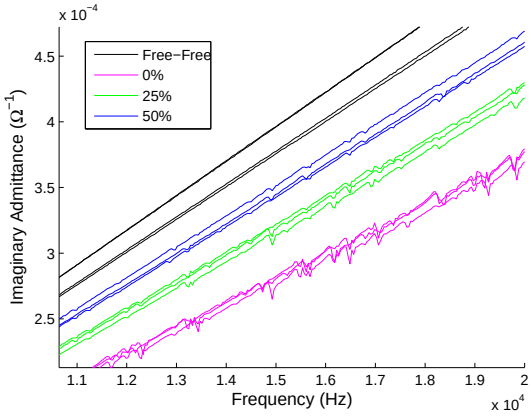

Figure 2.5: The variation of the signals decrease as with bonding percentage

Another characteristic of the signal that could be used determine the bonding condition is the amount of deviation that the imaginary admittance signal has from the slope. The variance in a specific signal, not the variance from one signal to the next, is caused by interaction between the PZT sensor and the structure, i.e. the resonances of the host structure. If Figure 2.5 is examined, a definite reduction in the variance of the signal can be seen from the fully bonded sensors (pink) to the free-free sensors (black). To quantify the reduction in variation, a least squares fit is performed on the imaginary impedance signal, then that line is subtracted out of the signal. What remains is the deviation from the overall slope of signal. If the standard deviation of the remaining signal is calculated, it can also be an indication of bonding condition.

Plots of standard deviation and bonding condition are found in Figure 2.6. When one examines the plots of the standard deviation of the various bonding cases, a definite reduction in the standard deviation can be seen. This reduction corresponds to a reduction in bonding percentage, and this reduction is caused by the reduced coupling between the structure and the PZT transducer from smaller bonding percentage. Under certain conditions, the standard deviation test might be useful as a second bonding condition test.

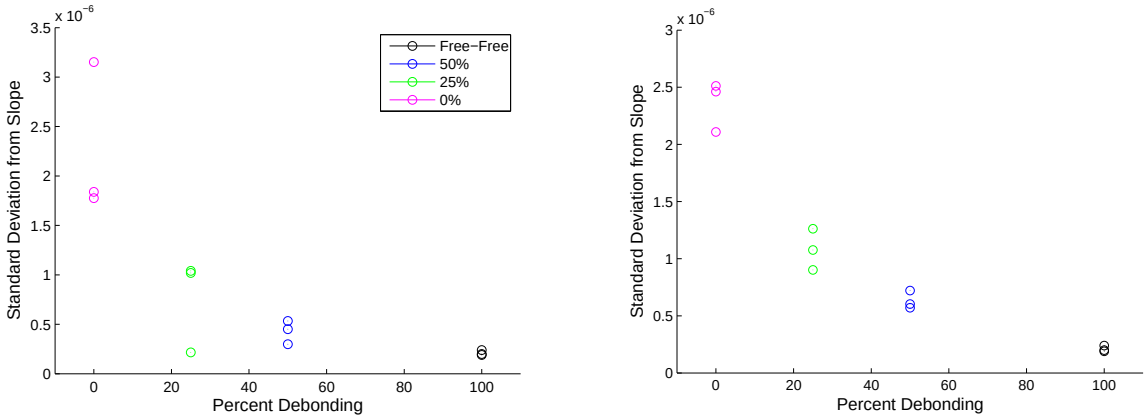

(a) Super Glue (b) Epoxy

Figure 2.6: The decrease in signal variation is correlated with bonding percentage

2.2.3 Wire Lead Detachment

To investigate the signals received from a patch that had a broken lead, two patches were bonded to an aluminum plate and the ground lead on one and the voltage line on the other were broken off at the patch. Various impedance measurements were then taken. This test was performed to verify that the PZT sensor that was damaged in this manner would not be confused with a healthy sensor on a damaged structure.

Two PZT patches were bonded to a 6.35mm thick aluminum plate. Both sensors are 12.7mm round PZT patches. The positive lead of one patch and the negative terminal on the other patch were detached by pulling the leads normal to the service. This caused the leads and a small part of the surface of the PZT sensor to become detached. The healthy and damaged PZT transducers can be seen in Figure 2.7.

Once the leads were removed, five different setups were tested to simulate the possible resulting locations that the wire leads could come to rest. The five possible locations for the lead to be located are the following:

1. Resting on the conductive aluminum plate.

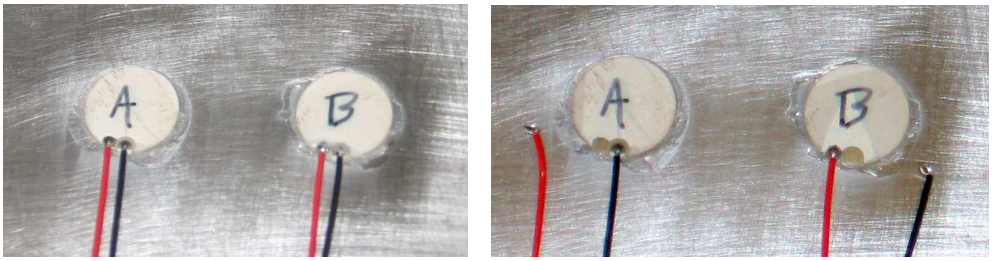

(a) Attached (b) Detached

Figure 2.7: The results of detaching the wire leads by pulling on the leads normal to the plate surface

2. Resting on the patch surface.

3. Resting on the patch breakage.

4. Hanging in a free state.

5. Resting on the other lead, creating a short.

These five conditions were tested with each patch. Patch A, in Figure 2.7(b), had the positive terminal detached, and its imaginary impedance measurements are shown in Figure 2.8. In this figure, the positive terminal detachment can cause three distinct signal changes. The first detachment case can cause the slope to drop to zero, which is when the end of the lead is in a position to create an open circuit. In Figure 2.8, the result of the open circuit is seen in the *Lead on Breakage* and *Lead Free* cases, their lines lie on top of one another and they lie on the x-axis. The second case is when the leads form a short and cause extreme variance and/or negative slope. The second case is shown in the *Lead on Lead* and *Lead on Plate* cases. The lead breakage can cause a third result, which is very similar to the undamaged case. This results happens when the positive lead rests in the *Lead on Surface* case. The only difference between this result and a signal from an undamaged sensor is the occasional drop in the imaginary admittance at random frequencies. This drop approaches the open circuit cases, and is probably caused by brief separations of the lead and patch. None of the above failure

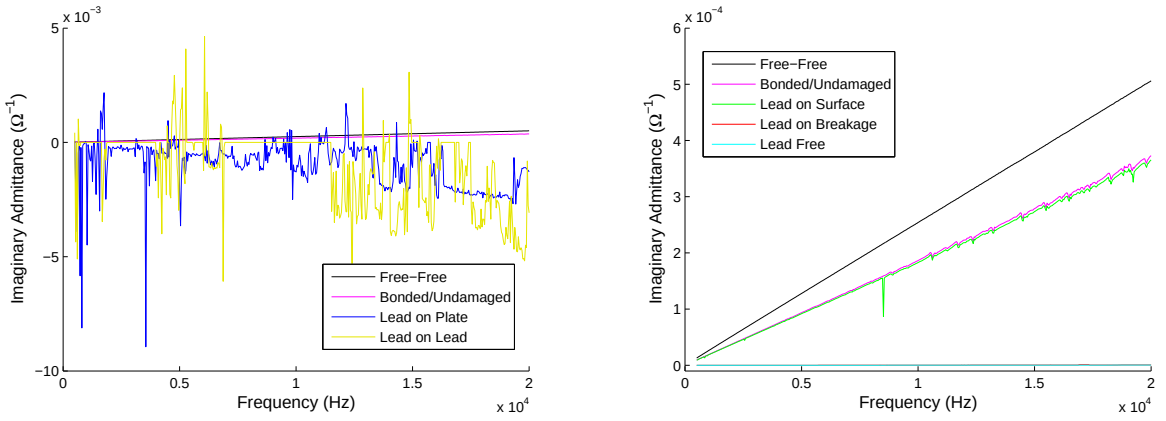

(a) (b)

Figure 2.8: For the positive terminal detachment (a) the Lead on Lead *and the* Lead on Plate *act as shorts and (b) the* Lead on Surface *acts similar to a fully bonded patch*

cases would indicate a false positive for structural damage; the cases would all be readily noticeable as sensor failure compared to the previous damage cases.

The negative terminal detachment reacted very similarly to the positive case. Figure 2.9 shows the results of the negative terminal detachment. This detachment has the same three possible results, as the previous test, but at different lead positions. In negative lead detachment scenario, the *Lead on Surface* acts as an open circuit, the *Lead on Lead* is the only short circuit, and the *Lead on Plate* acts similar to an undamaged patch. The other cases act as open circuits, just as before. The difference in the *Lead on Lead* case is due to a more consistent contact in the negative terminal detachment case. As with the positive terminal detachment, the results from this test indicate that this type of sensor failure will not be interpreted as structural damage.

It should be noted that it is unlikely that all types of piezoelectric patches will react the same way, but it is reasonable to assume that the three cases (open-circuit, short-circuit and appearing undamaged) could occur with any patch, although the combination of leads and locations may be different. The experimental investigation in Section 2.2 demonstrated that the susceptance signal does indicate sensor breakage and sensor debonding, and that the change in the slope is proportional to the amount of debonding or breakage that the sensor sustained.

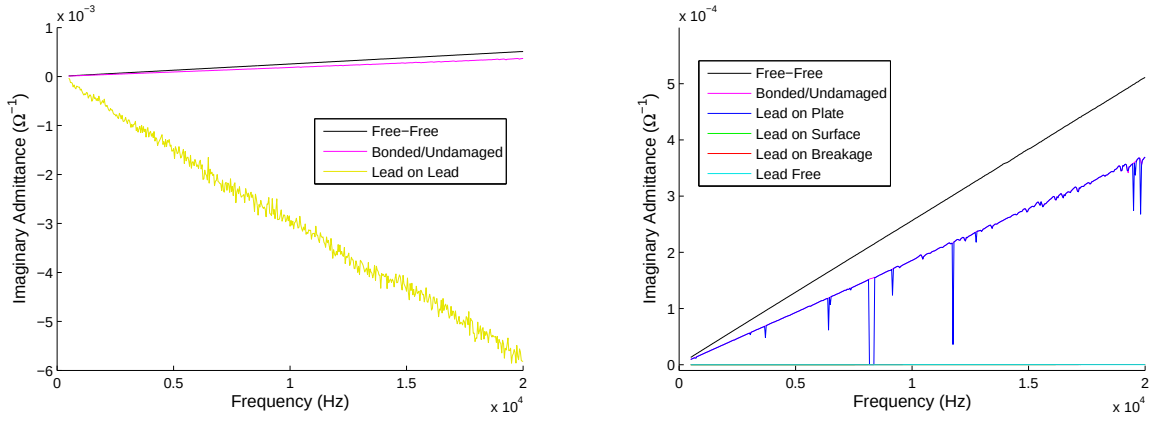

(a) (b)

Figure 2.9: For the negative terminal detachment (a) the Lead on Lead*acts as short and (b) the* Lead on Plate *acts similar to a fully bonded patch*

2.3 Effects of Temperature Changes

As temperature changes the physical properties of the structure, the bonding layer and PZT sensor will also change to varying degrees. The result is a shift in the imaginary admittance measurements made in the previous section. The extent of these effects is examined in this section. In order to make the sensor diagnosis procedure viable in a real world setting, temperature effects on the susceptance should be understood. Both broken and debonded patches were examined for the effect that temperature had on the susceptance for each failure mode.

2.3.1 Debonding

The test setup was the same 6.35mm thick aluminum plate with the debonded patches that were used in Section 2.2.2. In addition to the basic measurements, the plate was heated and impedance measurements were repeated at incremental temperatures. The plate was heated from room temperature to $135°F$, and the impedance measurements were taken from 500 to 20,000 Hz using an Agilent 4294A impedance analyzer. Once the imaginary admittance measurement was taken at each temperature, a linear least-squares fit was performed on the

measurement to obtain the slope of the signal. This slope value is what was compared among temperature values. The linearity of the signal should be checked before this fit is performed because some structures may have resonances within the frequency range causing an error in the slope value.

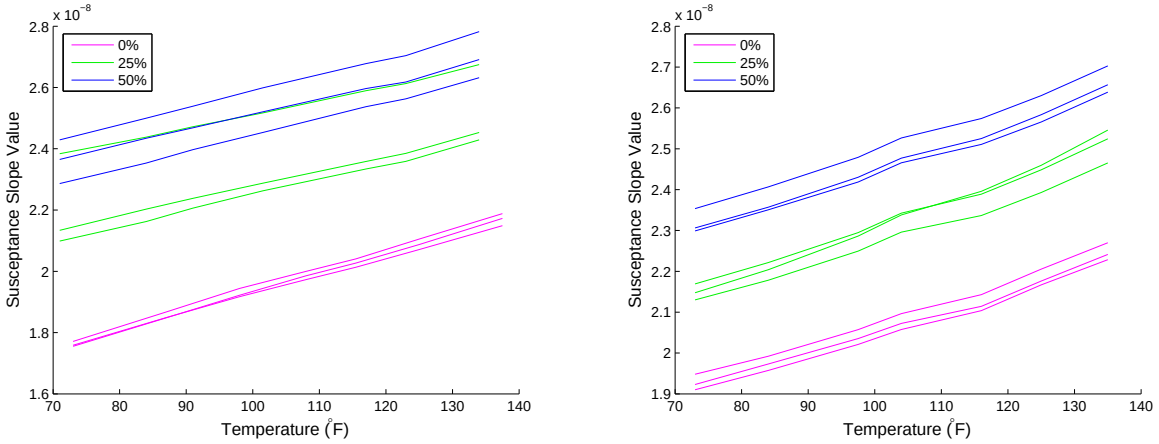

(a) Super Glue (b) Epoxy

Figure 2.10: The slope change of susceptance verse temperature for three different bonding percentages for both a) super glue and b) epoxy

The primary concern was that the slope of the susceptance would vary differently among different bonding and sensor conditions, thus making it more difficult to assess the bonding condition though the examination of the imaginary admittance slope. The results of the temperature test on debonded patches are shown in Figure 2.10. It can be seen in this graph that as temperature increases the capacitance value of the PZT transducer increases. It can also be seen that the patches bonded with epoxy and superglue have a similar slope change with temperature. From room temperature to a temperature of $135°F$ all the conditions that were bonded with epoxy and super glue had a $0.35e^{-8}$ increase in their slope value. Because of the parallel nature of the slope increase, a sensor diagnostic algorithm that is invariant of temperature changes should be developed. This algorithm could take advantage of this temperature independent characteristic of the sensors' susceptance signals though a method of outlier de-

tection.

2.3.2 Breakage

As an additional check, the effects of temperature on the susceptance measurements of broken patches were also examined. The procedure was the same as the debonding temperature test, but using the broken patches from Section 2.2.1. The results of the temperature test, performed on broken PZT sensors, are shown in Figure 2.11.

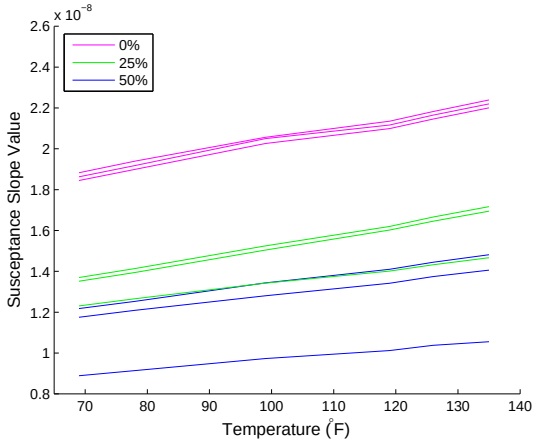

Figure 2.11: The slope change of susceptance verse temperature for various breakage percentages bonded with super glue

As with the debonded sensors the broken sensors behave in a predictable manner, with all of the breakage cases changing in a proportional manner. The change in both the debonded and broken sensor's susceptance signals indicates that temperature effects must be removed in a sensor diagnostic algorithm, because sensor failure and temperature changes alter the susceptance signal in a similar manner. The uniform change in various breakage percentages would allow for a temperature effects to be removed, if a method for outlier detection was used.

2.4 Conclusions

In this chapter the effects on the susceptance measurements of various types of PZT sensor failure were investigated. It was shown that the change in the imaginary admittance was proportional to the amount of damage or debonding the sensor experienced. There are several key aspects of admittance measurement that will make it useful in the active sensor validation role. The first is the low maximum frequency required for a meaningful measurement, which allows for the slope of the susceptance to be obtain with relatively few numbers of data points and, correspondingly, lower hardware requirements. The second benefit of admittance measurements is the lower power requirements of the technique, which allows for a more viable SHM system. The final benefit is the ability to find outliers in a sensor array at any temperature with no pre-stored baseline measurement required, allowing for sensor diagnostics without the need to collect training data. Because it was shown that certain kinds of sensor failure, debonding and breakage, can affect the SHM measurement in a way that resembles damage to the structure, sensor health must be taken into consideration when designing a robust SHM system.

Chapter 3

Effect of Sensor Failure on SHM Measurements

3.1 Introduction

PZT transducers are used to collect a variety of SHM measurements, including impedance measurements, Lamb wave propagation and frequency response functions (FRF's). The effect of sensor failure on these measurements was examined in this chapter. This additional testing was done to quantify the relative importance of healthy sensors in making those measurements. An important aspect of the sensor diagnostics is to determine the types of effects that various bonding conditions have on the different types of signals used in SHM. This testing will allow one to make a determination if a particular failure mode is of concern, for a given type of measurement being made. The three types of measurements investigated in this thesis are the impedance method, Lamb wave propagation and frequency response measurements. These measurements are examined because they are typically used with PZT transducers in the SHM field. Because of the types of easily distinguishable failure indicators that are received when a lead becomes detach, the effects of wire lead detachment on SHM measurements will not be examined.

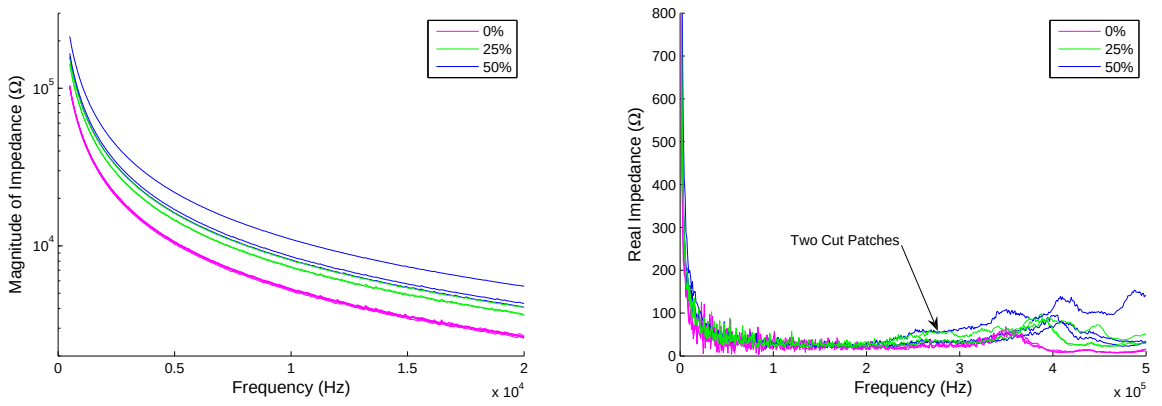

(a) Magnitude (b) Real

Figure 3.1: The effect of patch breakage on a) the magnitude measurement and b) impedance measurements over a wide frequency range

3.1.1 Impedance Measurements

The first of the SHM measurements to be examined for the effects of sensor failure is the impedance method. The first failure mode that will be discussed is PZT sensor breakage, then sensor debonding and finally wire lead detachment. The two main failure modes, breakage and debonding, will be examined for their effects on the impedance method for SHM.

Sensor Breakage

In the event of a PZT transducer breakage, there would certainly be a change to the characteristics of the transducer, and correspondingly the measurement it records. The overall area of the patch would decrease, and according to Equation 1.1, the impedance measurements would be scaled by a factor of the reduction in area. To measure this concept, the six 12.7mm PZT sensors, bonded to the 6.35mm thick aluminum plate used in Section 2.2.1, were also tested for these effects. The first plot, Figure 3.1(a), shows the effect on the magnitude of the impedance measurement from pre- and post-breakage. The breakage of the sensors caused a definite reduction in the magnitude of the impedance signal.

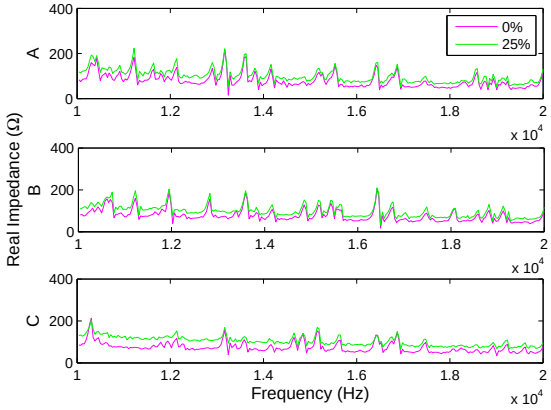

(a) 25% Breakage

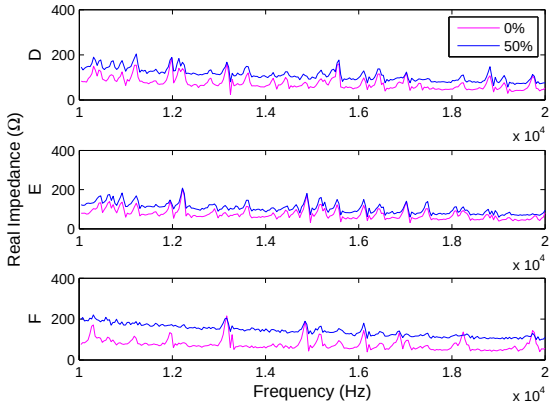

(b) 50% Breakage

Figure 3.2: The effect of breakage on impedance measurements over a narrow frequency range on a) 25% breakage and b) 50% breakage

The second type of impedance measurement that was examined for change was the real part of the impedance measurement. The real part of the impedance measurement is the part most commonly used for SHM. The specific signal that was recorded for comparison was a very broadband real impedance measurement, and appears in Figure 3.1(b). The broken patches did not develop obvious peaks or resonances in the impedance measurements, in fact they were largely unchanged. Two of the impedance measurements labeled in the figure did deviate from the undamaged case, but they were the patches cut with the abrasive wheel and the change is likely due to the damage to the aluminum plate caused by the cutting process.

The first low peak in the real impedance of the undamaged case that appears at approximately 350 kHz, does shift to a higher frequency after breakage. This peak is most likely a resonance of the PZT patch, and as the patch decreases in size, the frequency increases. However, SHM measurements should generally be made below the resonate frequency of the transducer, so that the dynamics of the structure and not the patch are measured.

Knowing that the breakage did not affect the broadband real impedance signal in a significant way allowed for the examination of whether or not a broken patch could still give meaningful information. To examine this possibility, two plots were generated showing a

real impedance measurement over a given frequency range for a patch prior to damage and after damage. Figures 3.2(a) and 3.2(b) show the results of the closer examination of the real impedance measurement of the broken PZT transducers. From the closer view of the impedance signal, a small but definite offset caused by the breakage, can be seen. The sensors broken with chisel (A,B,D and E), there are only slight changes in the shape of the real measurement, with some of the peaks being attenuated. The signals from the sensors cut with the abrasive wheel show a more significant change in the shape of the signal, most likely caused by the slight damage to the aluminum plate from the cutting process. From these two cases, it can be said that the ability to detect structural damage after PZT transducer breakage is situationally dependent. If the sensor is known to be broken, it is possible to take that into consideration when determining if the underlying structural dynamics have changed. Without the knowledge of sensor failure the slight changes in shape and magnitude would be interpreted as changes in the system, which would lead to a false positive interpretation of structural damage.

Debonding

The effect of bond condition should also be examined for basic impedance measurements. Active-sensing SHM relies on a good coupling between the patch and host structure for proper monitoring. The debonding of the PZT patch would affect the impedance measurement in a significant way, because of the coupling. The impedance of the sixteen 12.7mm PZT patches, which were bonded to a 6.35mm thick aluminum plate, were tested. These PZT transducers are the same ones used in Section 2.2.2, and were bonded with 0, 25 and 50 percent debonding, with both super glue and epoxy. The impedance was measured over the widest possible useable range for impedance measurements, from 500 Hz to 500 kHz [16]. The results are shown in Figure 3.3.

It can be seen that the debonding of the patch has caused the real impedance to have very distinct peaks, and is because the response is now dominated by the characteristics of the PZT

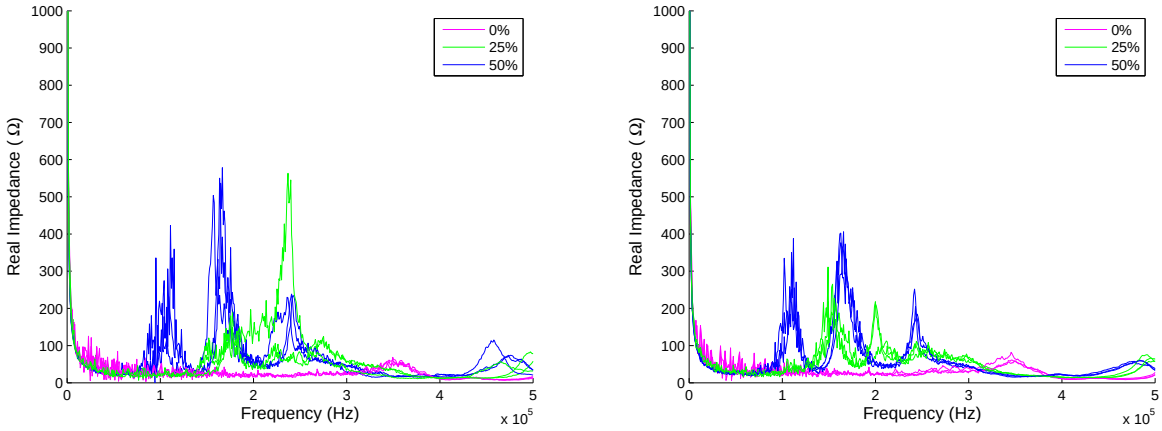

(a) Super Glue (b) Epoxy

Figure 3.3: The effect of debonding on impedance measurements over a wide frequency range on a) super glue and b) epoxy

patch and not the impedance of the structure. If the PZT patch were to become debonded at some time during service, there would be no way to determine whether or not damage had occurred in the area of the resonance frequency, because any change in the structure's impedance signature would be overwhelmed by the resonance of the PZT sensor. However, it may be possible, if the patch was initially bonded with an imperfect bond, to still make meaningful SHM measurements. It is not known if changes in the system can be detected with a partially debonded sensor, if the baselines were taken with the identically debonded sensor on a healthy structure. If changes could still be detected in such a situation, it would allow for damage detection even when the absolute bonding condition could not be assessed. The possibility for damage detection under these circumstances is examined further in Chapter 4, where the sensor diagnostic algorithm is discussed.

3.1.2 Lamb Wave Propagation

When a Lamb wave is excited in a plate it travels in all directions from that point. When the waves contact an edge or damage, they are reflected. The direct signal and reflection are

recorded and analyzed. Any damage in the sensor could be mistaken as damage in the structure depending on its effect to the signal. The signal that is recorded has three main regions. These regions can be seen in Figure 3.4. The first is the *Interference* region caused by the electrical excitation of nearby patch. The *Direct Wave* region is the signal that traveled directly to the sensor through the plate, and the *Reflections* region is composed of waves that arrive from indirect sources. To investigate the affect of sensor failure on Lamb wave propagations, both of the primary sensor failure modes were examined: debonding and breakage.

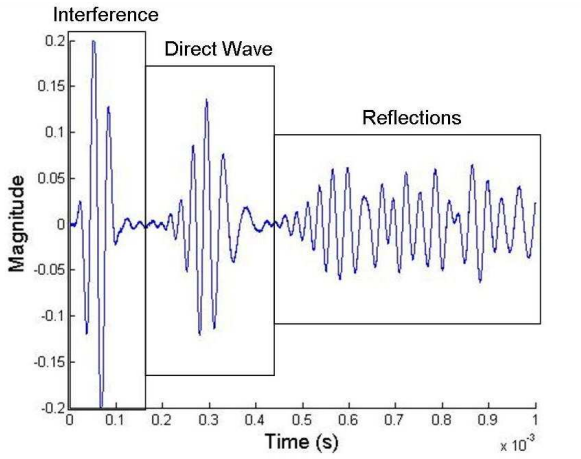

Figure 3.4: A Lamb wave measurement has several distinct regions

The test setup used to test the effects of both debonding and breakage was a plate with nine 12.7mm round x 0.2mm thick PZT sensor/actuators bonded to it. All sensors were bonded with super glue. This aluminum plate was 122cm x 122cm and was 1.6mm thick. The PZT sensors were placed on a grid of 3x3 equally spaced in the center of the plate. A picture of the plate is shown in Figure 3.5.

To assist in selecting the proper excitation frequencies, the dispersion curves for a 1.6mm thick plate were calculated, and are shown in Figure 3.6. These curves are similar to the examples given in Figure 1.3, but are specific to this aluminum plate with a thickness of 1.6mm. Four frequencies were selected for excitation: 30, 50, 100 and 200 kHz. The 100 kHz region

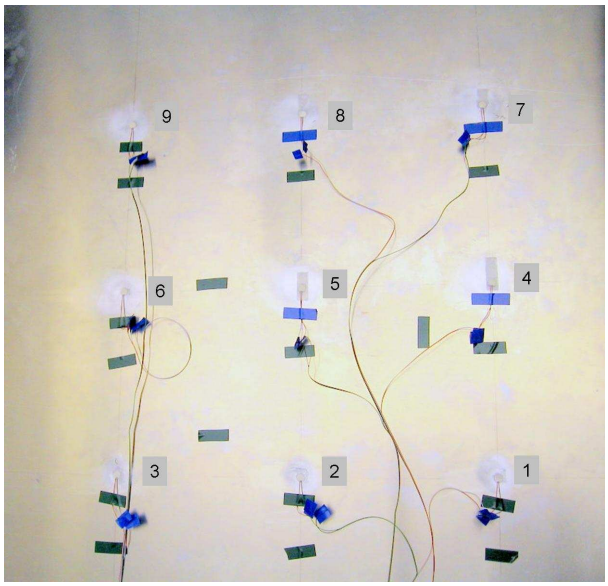

Figure 3.5: The sensor array used to measure the effects of sensor failure on Lamb waves

falls directly in a resonance pattern for a 50 percent debonded PZT sensor shown in Figure 3.3(a), and was selected to help test this possibility.

Sensor Breakage

To test the effects of patch breakage, two transducers from the initial bonding condition were broken. The patches that were broken were numbers seven and nine from Figure 3.5. These two sensors allowed for the testing of various signal path lengths with the two different PZT transducers. Sensor number seven was broken in an irregular pattern to simulate a more real world failure, while sensor number nine was broken at a 50 percent line. Both of the transducers are shown in Figure 3.7

The first step before testing could begin was to verify that the bonding conditions of the PZT patches were consistent on the plate. An impedance measurement was taken on each of the PZT transducers after damage was inflicted. The results are shown in Figure 3.8(a), which shows that the damaged PZT sensors underwent a decrease in their imaginary admittance

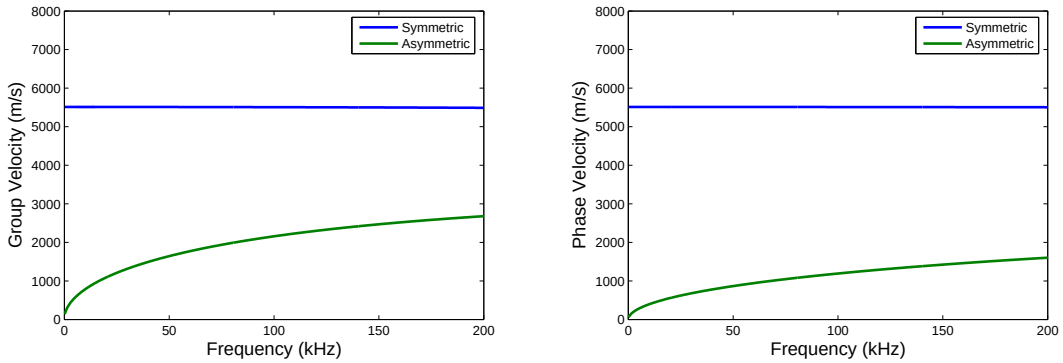

(a) Group Velocity (b) Phase Velocity

Figure 3.6: Specific dispersion curves for a 1.6mm thick aluminum plate

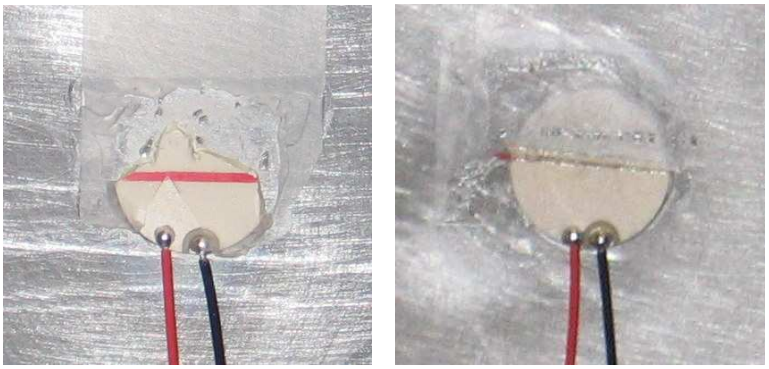

(a) Irregular Breakage - Patch 7 (b) 50% Breakage - Patch 9

Figure 3.7: Pictures of the two broken PZT transducers used to test the effect of sensor breakage on Lamb wave propagation

slopes. This change is consistent with previous observations about patch breakage.

The next step is to examine the actual Lamb wave measurements. A plot of the direct wave region, of two different path lengths at a variety of excitation frequencies, is given in Figure 3.9. The two different lengths of *short* and *long* correspond to a 30.5cm path length and a 61.0cm path length respectively. An example of a short path length in Figure 3.5 would be from patch one to patch four, and a long path length would be from patch one to patch seven. Four excitation frequencies were used to obtain a wider spectrum of results and to check for

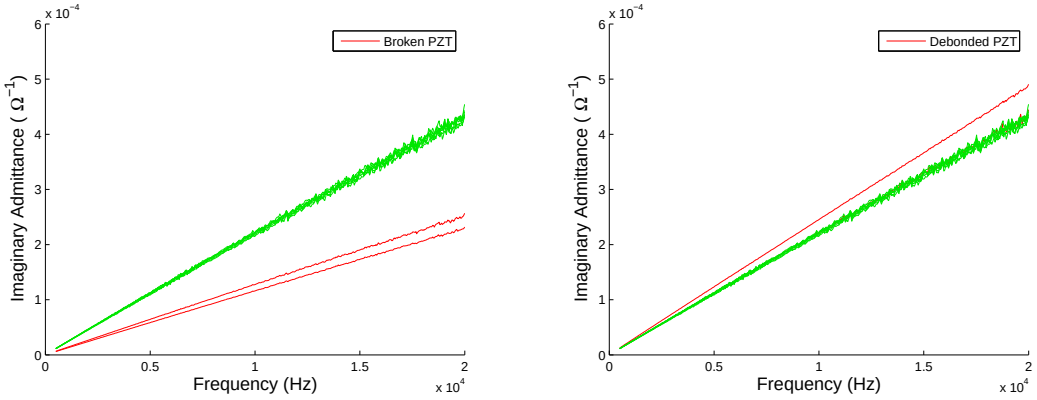

(a) Breakage (b) Debonding

Figure 3.8: The imaginary admittance of PZT sensors decrease after breakage and increases after debonding

consistency among different excitation frequencies. The four excitation frequencies of 30, 50, 100 and 200 kHz can be seen in Figures 3.9 and 3.10. All possible *short* and *long* paths were recorded and shown.

The effect of a broken PZT transducer is an attenuation of the signal at all excitation frequencies, with slight phase differences at certain frequencies. The attenuation is expected because a broken sensor will have less area that will pick up the signal, so it will experience less strain and produce less of a voltage output. The attenuation and phase differences are most severe at the higher two frequencies of 100 and 200kHz, but are present at all frequency, and are the most severe between the two broken sensors. The changes in the signal at all frequencies could be interpreted as damage to the structure without sensor validation.

Debonding

The second sensor failure mode to be examined with regards to Lamb wave propagation was sensor debonding. To facilitate this test, the two broken transducers from previous experiment were removed and two healthy, but partially bonded, transducers were bonded in their

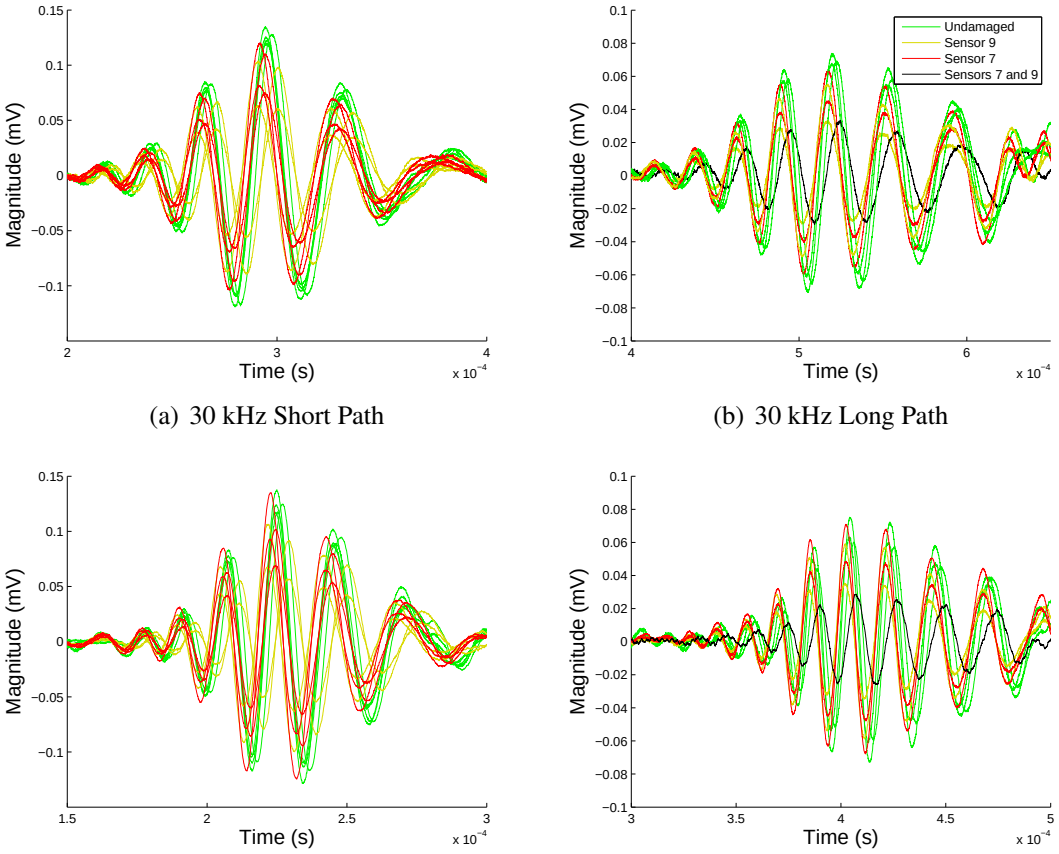

(a) 30 kHz Short Path

(b) 30 kHz Long Path

(c) 50 kHz Short Path

(d) 50 kHz Long Path

Figure 3.9: The effect of broken PZT sensor number seven (red), number nine (red) and both nine and seven (black) a on a pitch-catch Lamb wave measurement of two different lengths for 30 and 50 kHz excitation

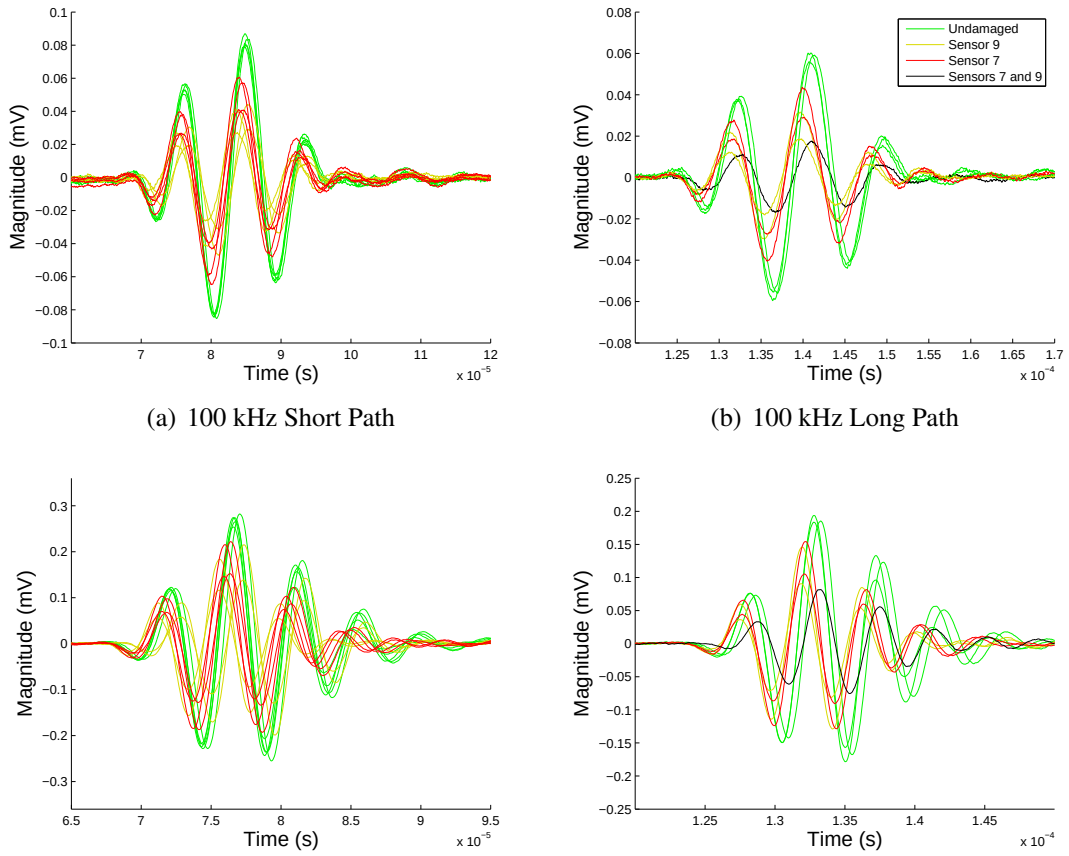

(a) 100 kHz Short Path

(b) 100 kHz Long Path

(c) 200 kHz Short Path

(d) 200 kHz Long Path

Figure 3.10: The effect of broken PZT sensor number seven (red), number nine (red) and both nine and seven (black) a on a pitch-catch Lamb wave measurement of two different lengths for 100 and 200 kHz excitation

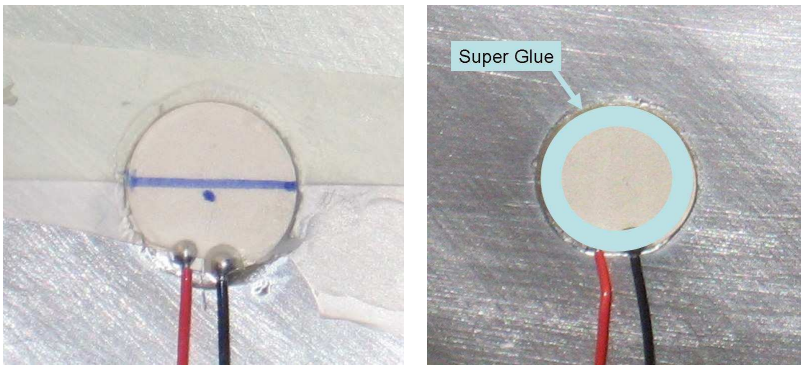

(a) 50% Debonding - Patch 7 (b) Center Debonding - Patch 9

Figure 3.11: Pictures of the two partially bonded PZT transducers used to test the effect of sensor debonding on Lamb wave propagation

place. One PZT patch was bonded at 50 percent debonding, while a second was bonded with a perimeter bonding pattern. A picture of both PZT patches can be seen in Figure 3.11.

After the two PZT patches were bonded in the seven and nine positions from Figure 3.5, the imaginary admittance measurements were taken to verify bonding conditions. The results from this test are shown in Figure 3.8(b). From this plot, it can be seen that the 50 percent debonded patch has a significant increase in the slope of the imaginary admittance; however the perimeter bonding indicates that it is bonded as well as any of the other sensor/actuators on the aluminum plate. The lack of change in slope indicates that the measurements taken from that PZT sensor should be as good as the remaining patches.

As with the transducer breakage, the Lamb wave measurements were examined next. Two path lengths were again examined to test the effects of the PZT debonding on the Lamb waves.

It is shown in Figures 3.12 and 3.13 that the most significant changes in the Lamb waves are caused by paths that contain the PZT transducers located in position seven. This transducer is the one with 50 percent debonding. Depending on the excitation frequency, the signal can be attenuated, similar to the broken case, or amplified. The amplification is a result of the resonance frequency being similar to the excitation frequency. In addition to the amplification

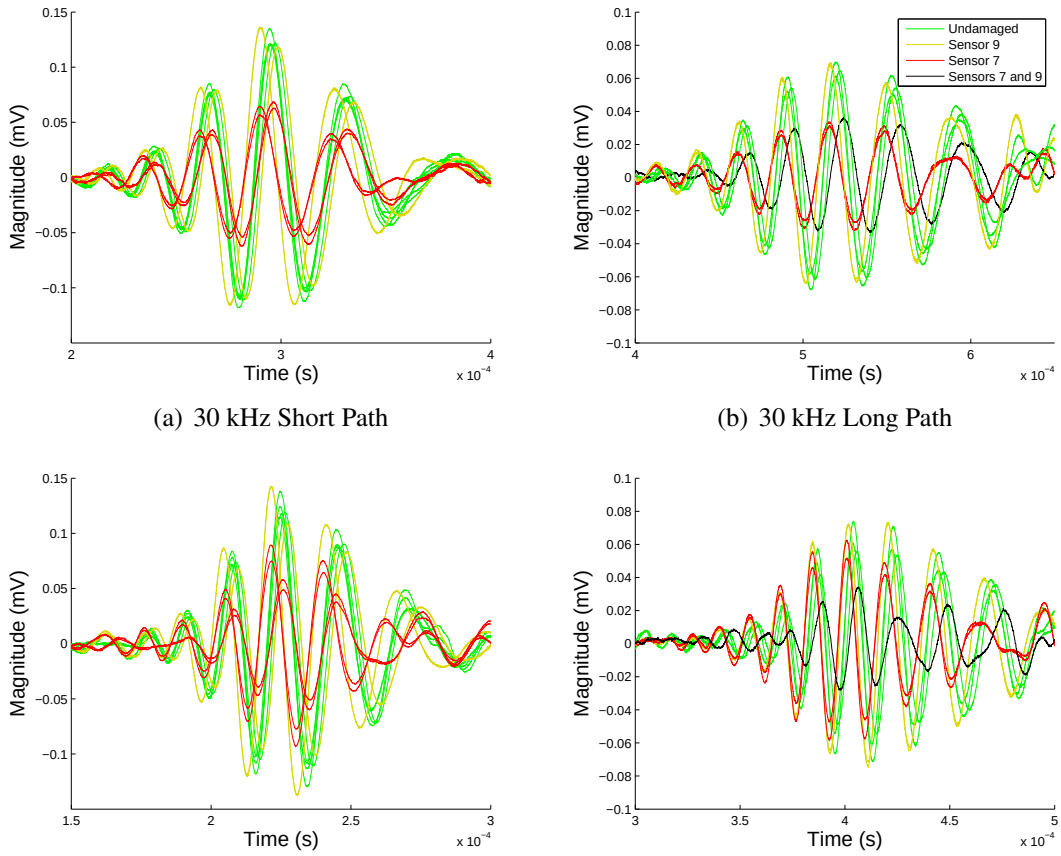

(a) 30 kHz Short Path

(b) 30 kHz Long Path

(c) 50 kHz Short Path

(d) 50 kHz Long Path

Figure 3.12: The effect of debonded PZT sensor number seven (red), number nine (red) and both nine and seven (black) a on a pitch-catch Lamb wave measurement of two different lengths for 30 and 50 kHz excitation

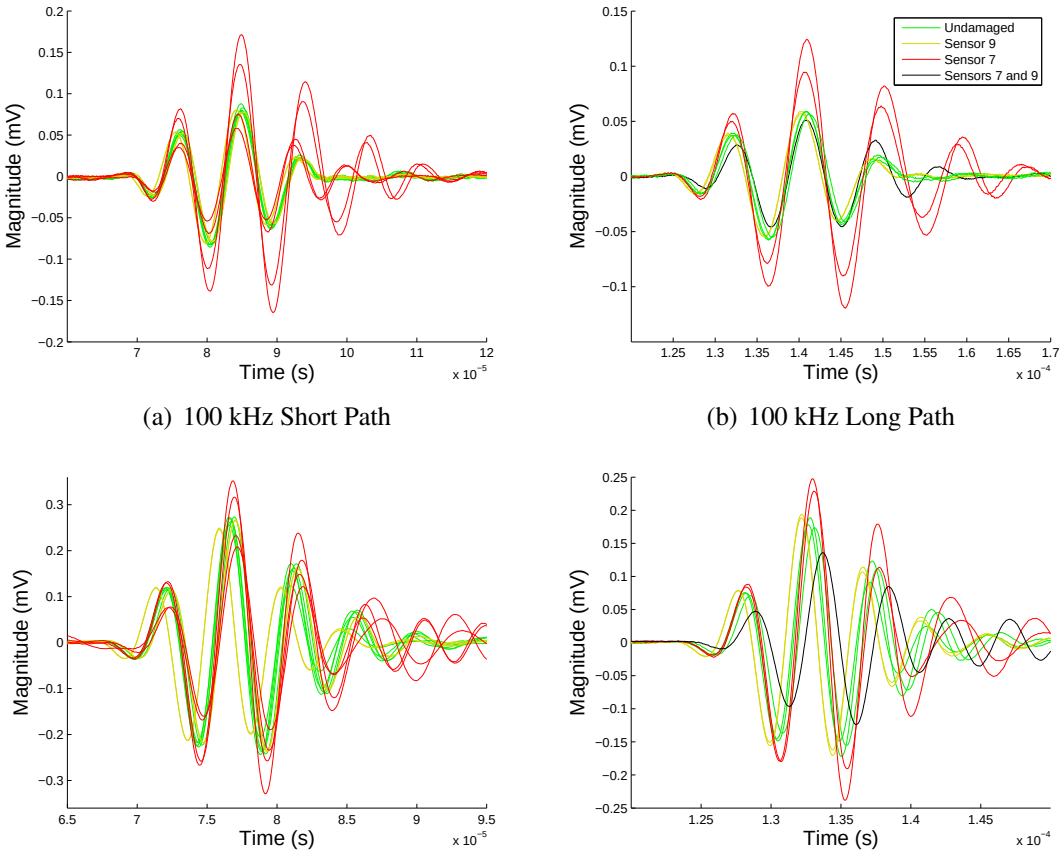

(a) 100 kHz Short Path

(b) 100 kHz Long Path

(c) 200 kHz Short Path

(d) 200 kHz Long Path

Figure 3.13: The effect of debonded PZT sensor number seven (red), number nine (red) and both nine and seven (black) a on a pitch-catch Lamb wave measurement of two different lengths for 100 and 200 kHz excitation

or attenuation to the signal, there is also a shape change to the wave. This shape change is most evident in the trailing portion of the wave, and can be seen as a phase difference from the undamaged signals. To reinforce the validity of the imaginary admittance sensor diagnostic measurement, PZT transducer number nine has no appreciable effect on the resulting Lamb wave propagations.

3.1.3 Frequency Response Functions

PZT sensors are sometimes used to obtain frequency response functions. The same 122cm x 122cm and 1.6mm thick aluminum plate used in Section 3.1.2 was used for the FRF testing. PZT transducer number seven was used to measure the FRF with an input signal sent from sensor number eight. The signal was averaged fifty times with a Hanning window applied. A healthy, 50 debonded and a 50 percent broken PZT transducer were all tested at location number seven. From these measurements, two plots were generated of the effects of the two primary sensor failure modes on frequency response functions. Sensor breakage is shown in 3.14(a) and 3.14(b) and the effect of debonding is shown in Figure 3.14(c) and 3.14(d).

By comparing the results in the close up views seen in 3.14(d) and 3.14(b) it can be clearly seen that the main effect of sensor failure is a reduction in the magnitude of the FRF. The attenuation is not equal in its affect on every mode in the system; some frequencies are reduced more than others. Depending on the use of the FRF, this attenuation can be an issue. If the magnitude of the response is being used for some purpose, then sensor failure would largely affect those results, and any direct comparisons being made. For example, if damping was being measured, this change would be significant. The natural frequencies of the system are reasonably stable, but some of the content does shift slightly. These effects were measured in the lower frequency range, and would certainly be amplified in the higher frequency ranges in the region of the sensor resonance.

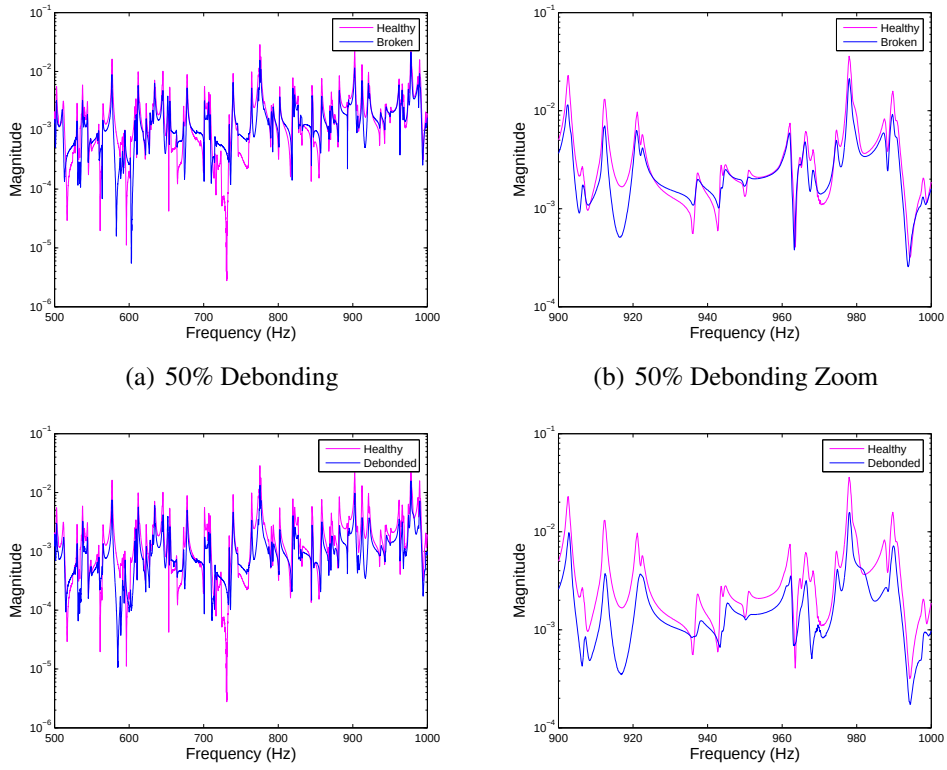

(a) 50% Debonding

(b) 50% Debonding Zoom

(c) 50%Breakage

(d) 50% Breakage Zoom

Figure 3.14: The effect sensor failure is an attenuation of the FRF magnitude

3.2 Conclusions

In this chapter the effects of sensor failure on SHM measurements was investigated to better understand the importance of sensor diagnostics. In general, the sensor failure produces the significant changes in magnitude and shape to the SHM measurements. These feature are the same two that are often examined in SHM to detect damage in a system. Because of the similarity of these features, sensor diagnostics is a necessary component in a robust SHM system to avoid the false-positive prediction of damage in a structure when only sensor failure has occurred.

Chapter 4

Signal Processing Tools for Sensor Diagnosis

4.1 Introduction

Methods for specifically determining the health of piezoelectric patches have been examined in previous research, and are reviewed in more depth Chapter 1. A couple of the techniques specifically make use of the impedance measurements of the piezoelectric patch, although in different ways. Saint-Pierre et al. [31] uses the shape of the first real impedance resonance and its change to determine the state of the bonding condition. Guirgiutiu and Zagrai [13] propose a similar technique using the attenuation of the first imaginary impedance resonance for damage detection. Pacou et al. [32] discusses the use of the shift of the first natural frequency of the piezoelectric patch before and after bonding as a possible method for determining bonding condition.

There are several disadvantages to the above piezoelectric specific methods. First, they are not sensitive to small debonding in the PZT transducer and sensor fracture could cause the resonance to move beyond the monitoring region. Secondly they all require relatively high frequency measurements to determine the bonded first natural frequency. A standard impedance analyzer can be used to make a measurement into the 600 kHz range and up, which

is needed in these methods. Current SHM nodes that are used for the impedance based SHM are not able to make impedance measurements into that range [25]. This frequency requirement makes these techniques generally unsuitable for field deployment using currently available sensor nodes. Finally the absolute number of data points that need to be collected for sensor diagnosis is quite high compared to the method proposed in this paper. The higher number of data points demands more from the SHM node, which generally have very limited storage capacity and RAM.

Bhalla and Soh [10], in addition to the formulations in Section 1.2.1 suggest that the imaginary part of the admittance measurement is more sensitive to bonding conditions, and therefore could be useful in determining the bond health. This relationship was further developed by Park et al. [17, 6], who showed the initial relationship between bonding condition and the slope of the imaginary admittance measurement (susceptance).

From the introduction section on sensor diagnostics in Chapter 1, Equations 1.7 and 1.8 show that the same PZT transducer will have a different admittance measurement by changing from a free-free condition to a surface-bonded condition. The bonding of the sensor would cause a downward shift in the electrical admittance of the free PZT transducer by a factor of $d_{31}^2 \bar{Y}_p^E$. This change in slope would allow for the health of the bonding condition to be assessed with a measurement of the susceptance [6]. It is this characteristic along with the specific knowledge gained in Chapter 2 of how different failure modes effect the susceptance measurement that is developed into a robust sensor diagnostic procedure in this chapter.

4.2 Signal Processing Tools for Diagnosing the Health of Sensor Arrays

In this method, a procedure that uses the measured susceptance values of PZT transducers to allow for the state of the transducers to be obtained without the need for pre-stored baseline measurements is proposed. When a group of sensors is bonded to a similar structure, there is the opportunity to compare one sensor to another. This comparison can occur because the sensors are all exposed to the same environmental conditions and so those effects can be removed. Through a process of outlier detection, sensors with errant bonding or health conditions are identified, even in the presence of temperature changes.

For an array of sensors, the task lies in determining which of the sensors is not part of the healthy group. The algorithm takes advantage of the characteristic that the removal of an unhealthy patch will cause a greater decrease in the standard deviation of the group of sensors than will the removal of a health sensor. A process was developed to test the effect each sensor had on the overall standard deviation of the group of signals, and to determine at what point the change occurred from unhealthy to healthy sensors. This process is documented here:

1. The slope of each of the PZT transducer's susceptance signals, which is a measure of the capacitive value, is calculated in a least-squares manner.

2. The transducer in the group that contributes, by its removal, to the maximum reduction in the standard deviation is found.

    (a) One of the PZT transducer's susceptance signals is removed and the remaining group's standard deviation is recalculated.

    (b) The PZT transducer with the maximum influence on the standard deviation is recorded and removed from future iterations.

(c) Steps 2a and 2b are repeated until two sensors remain.

3. The sensors are arranged and plotted in descending order of influence.

4. The sensor that corresponds to the maximum distance from the total change is determined, and is recorded as the sensor that starts the healthy patches. The sensors with a greater influence than this patch are determined to be unhealthy.

A visual representation of the results from Step 3 are shown in Figure 4.1. The values that are plotted in this figure are the standard deviations of the slope values. Each point includes the admittance values of itself and all sensors to the right of it. For example, the point for sensor 7 in Figure 4.1 is the standard deviation of the admittance slopes from sensors 1 through 7.

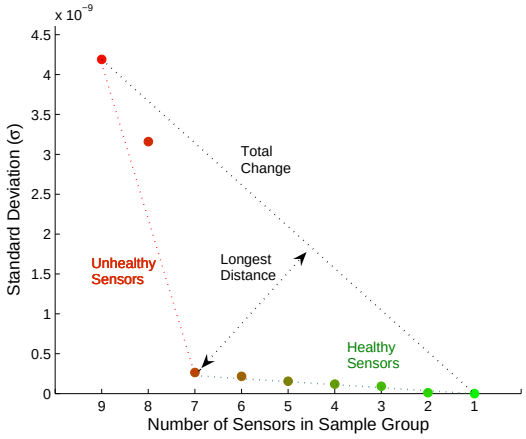

Figure 4.1: The longest distance from the overall change corresponds to the change from unhealthy to healthy patches

A couple rules were also implemented to increase the robustness of the procedure. The first rule is that the maximum number of recommend unhealthy patches is limited to less than half of the total number of sensors, which is implemented because a base group of sensors is needed for outlier detection. The second rule is that if a sensor's effect on the standard deviation is negative (it falls above the overall slope change), no sensors are recommended

for replacement, because the total slope change does a reasonable job at approximating the individual slope change. Although not a rule, the frequency range that is used in determining the slope of the susceptance should be examined to make sure there is no major structural resonance that would induce error into the least squares fit of the line.

A MATLAB script was written to implement the above procedure. As an initial test two plate structures that had 12.7mm PZT sensors bonded to them were examined. The first plate was a 1.6mm thick aluminum plate that measured 122cm x 122cm. This plate is shown in Figure 4.2(a), and has very uniform properties. Other structures may have a slightly higher variance due to structure irregularities. To investigate this possibility a second plate was examined that was 13mm thick and had aluminum honeycomb structure. The second plate measured 61cm x 61cm and it is shown in Figure 4.2(b). Each of the plates had sensors initially bonded to them, with varying degrees of health.

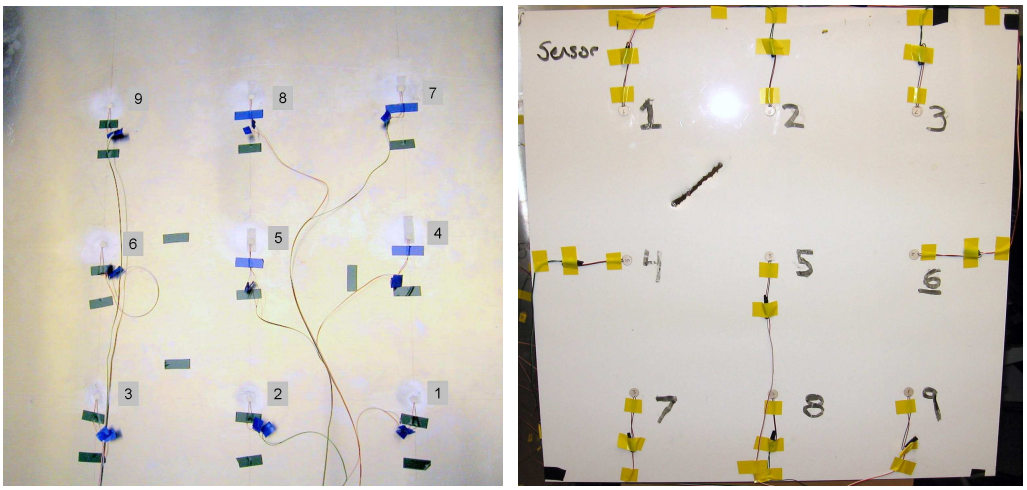

(a) 1/16” Aluminum (b) Aluminum Honeycomb

Figure 4.2: Two plates with poorly bonded patches were used to test the sensor array diagnostic algorithm

The sensor diagnostic algorithm was run on each plate. The output of the proposed algorithm is a hybrid plot with the upper plot showing all of the susceptance measurements with

color coding corresponding to the lower plot. The lower plot shows the effect of reducing the sample number, with the x-axis showing which sensor numbers are recommended for removal. The lower plot also has a line delineating the healthy patches from the unhealthy ones. The results from Plate 1 are shown in Figures 4.3(a) and 4.3(b) and the results from Plate 2 are shown in Figures 4.3(c) and 4.3(d). When the algorithm was run on each plate, several sensors on the solid aluminum plate were recommended for replacement and one sensor on the honeycomb plate was recommended for replacement. Those sensors were replaced and the algorithm was run again on each plate. Both plates passed the algorithm the second time. It should be noted that the honeycomb plate does have a grouping of values due to the heterogeneous nature of the material. The grouping of values shows the basic assumption, that the structure's impedance is vastly greater than that of the PZT transducer, is partially wrong. In this case, the thinness of the aluminum skin on the plate combined with the relatively stiff honeycomb structure does effect the susceptance measurements.

The main advantage of looking for the change in the data in this manner is that no absolute value for the effect of a sensor is required. The lack of a required pre-stored baseline allows this system to be used on a variety of structures with no training set required. A further test of the procedure was performed by bonding a sensor on each of the plates at a 50 percent bond area. The sensors were bonded on each plate at the number seven location, and were bonded in the same manner as is shown in Figure 2.3(c). Admittance measurements were taken with all the healthy sensors from Figures 4.3(b) and 4.3(d) except the debonded PZT sensor located at position number seven. The resulting measurements are shown in Figure 4.4. From the two plots the algorithm correctly identifies the poorly bonded PZT transducers on the solid aluminum plate and the honeycomb plate.

In order to compensate for temperature and environmental effects it is proposed that multiple sensors should be used in a given SHM system whenever possible. These extra sensors provide redundancy for measurements and allow for an efficient and reliable method for sensor

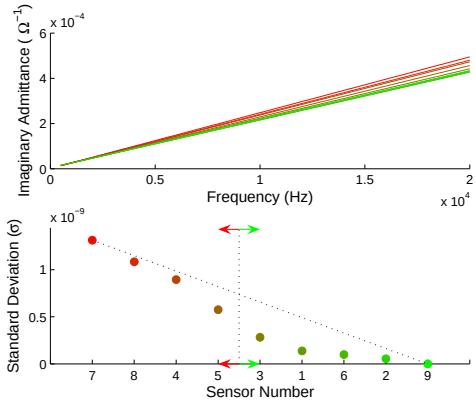

(a) Aluminum - Initial Condition

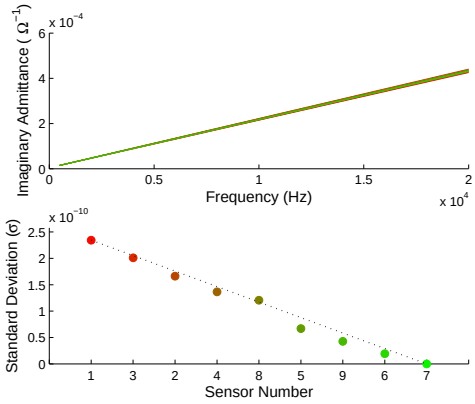

(b) Aluminum - Rebonded Unhealthy Sensors

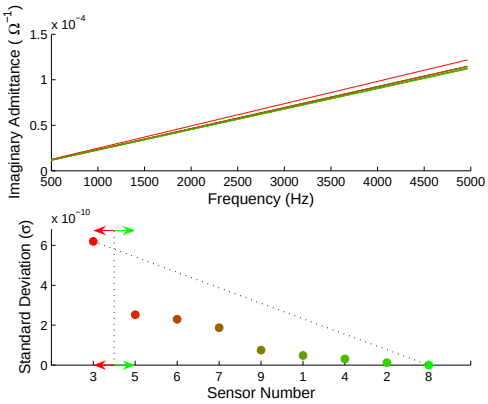

(c) Honeycomb - Initial Condition

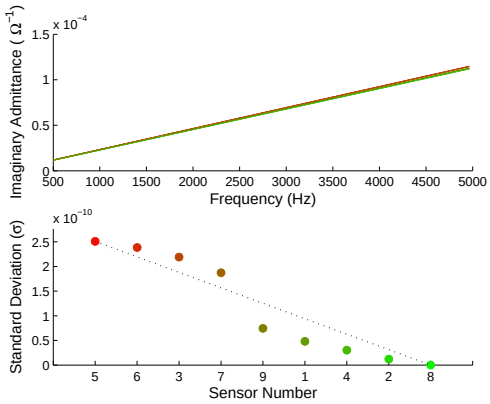

(d) Honeycomb - Rebonded Unhealthy Sensors

Figure 4.3: Each plate passes the sensor test after the recommended unhealthy sensors are removed and new sensors are bonded in their place

diagnostics. The imaginary admittance slope comparison will work with a group of sensors. Even during temperature changes, all the sensors will shift the same percentage for any given temperature change, as seen in Section 2.3. Care does have to be taken to make sure that the sensors being analyzed are exposed to the same environmental conditions, or false positives may occur.

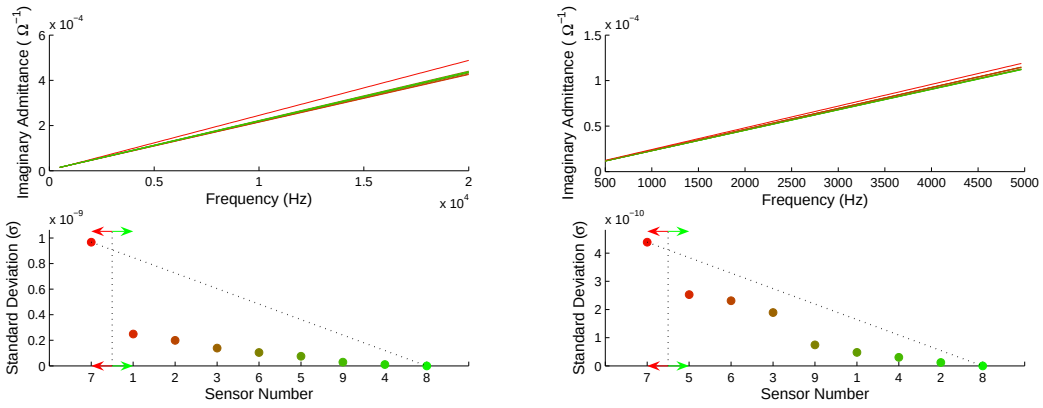

(a) 1/16" Aluminum

(b) Aluminum Honeycomb

Figure 4.4: The algorithm correctly identifies the debonded sensor on the solid plate and over estimates the number of damaged sensors on the honeycomb plate.

4.3 Algorithm for Single Sensors

The methods for single sensors prove to be a more difficult task, because there is no way to compare the results from one sensor to another sensor in the same situation. However it is often the case, that when there is not an array of sensors, that there still may be multiple sensors bonded in a similar manner. For example, a similar bolted joint could be monitored in several places on a structure. This similarity may allow for the measurements to be compared. If there is no similarity, or there is no possibility for additional sensors to be installed for redundancy, as recommended above, then a technique other than outlier detection will be needed.

It has been shown in Chapter 3 that an inconsistent bonding condition can effect both Lamb wave propagations and impedance measurements in a manner that is very similar to that of a damaged structure, but the same may not be true in single sensor applications. In single sensor impedance applications there is no patch to patch consistency required. It may be possible to detect changes in the system with a partially debonded sensor. The question is, does the bonding condition need to be perfect or is it acceptable to be consistent with whatever bonding condition exists for single sensor impedance measurements.

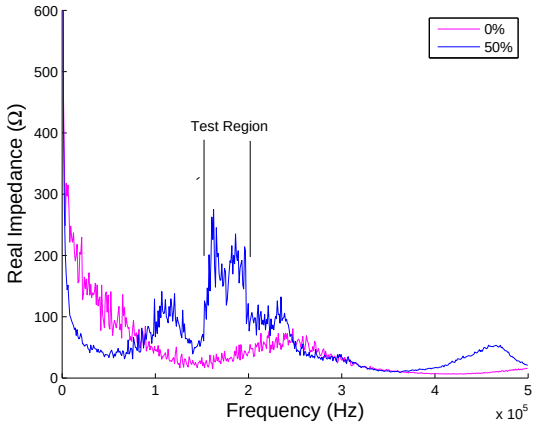

Figure 4.5: The region that had a large response due to patch debonding was used to test damage detection ability

To test this idea, a patch was bonded with 50 percent debonding to 1.6mm thick aluminum plate. The resonance of this PZT transducer was found, by examining the real impedance measurement shown in Figure 4.5. Two bands were chosen within the resonance peak, and were 160-170 kHz and 190-200 kHz. Five impedance measurements, in each band, were taken prior to damage and five measurements were taken after damage was introduced. Five measurements were used to account for variations in the signals. The measurements were then shifted positively or negatively in the frequency range up to 60 Hz to account for environmental shifts.

The response of the two frequency bands are shown in Figure 4.6. These plots show the two ranges in their entirety and a close up view of each one. It can be seen that the signal does change in both regions after damage was introduced. The signals do shift positively or negatively with temperature, but the before and after damage show a different shape even after the temperature effects are removed.

These results show that even in the region of sensor resonance, changes in the structure can be detected, if the sensor condition remains constant. The results also show that if the situation is completely unique, in that there is only one patch with a unique bonding condition,

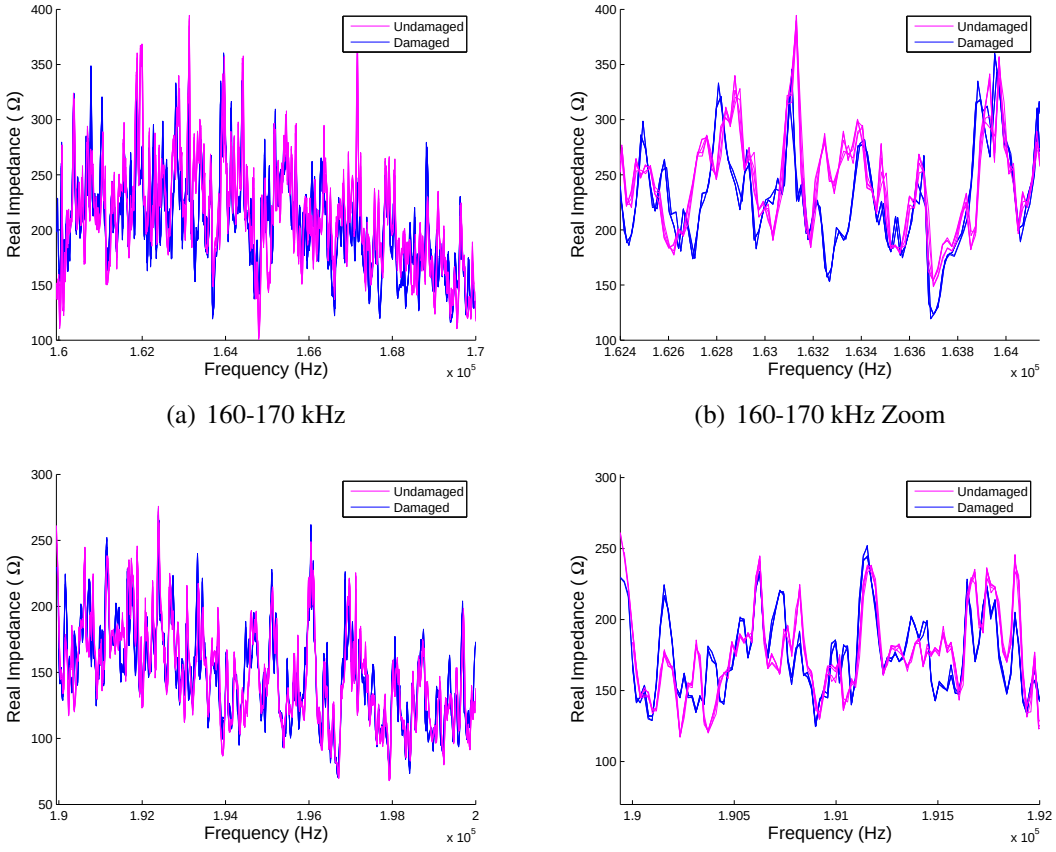

(a) 160-170 kHz

(b) 160-170 kHz Zoom

(c) 190-200 kHz

(d) 190-200 kHz Zoom

Figure 4.6: Two separate regions from the wide frequency band were examined for the change in signal before and after damage

a temperature reading must be taken. Although it is not done here, a regression analysis or a simple table of past measurements would be required to determine whether or not the bonding condition has changed. Once the bonding condition has been verified, then the current measurement could be compared to the previously stored base line measurement, and damage to the structure could be assessed. Temperature measurements at a modern microprocessor sensor node are easy to implement, requiring little power and few components. The main drawback is the need for time and opportunity to obtain the baseline measurements, which could be hard to obtain on large or sensitive structures. There is also an additional data storage requirement for the baseline measurements.

Although damage could be detected with a partially bonded sensor, it does not mean that it should be done. A partially bonded sensor will have a shorter life span and be more susceptible to damage. A known debonded sensor should always be replaced when possible, to insure the most reliable measurement.

4.4 Conclusions

The imaginary impedance measurement shows a great deal of promise for use in the structural health monitoring field as sensor diagnostic measurements. The method can be readily used with sensor arrays with no pre-stored baseline measurements, and potentially with single sensors with baseline measurements. The method can also distinguish between sensor breakage and sensor debonding and give relative percentages of each. In addition, impedance based measurement in the lower frequency ranges proposed here are more easily implemented with currently available hardware and have lower power requirements than other methods. Future work on the method should include a refinement of the single sensor procedure to include a robust regression technique, or the search for a temperature independent feature of the impedance measurement.

Chapter 5

Hardware Development for Sensor Diagnostics and SHM

5.1 Introduction

This chapter documents the development of an extremely compact, power-efficient impedance sensor node that can be used in structural health monitoring and sensor diagnostics. The device is part of the integrated hardware and software solution for SHM that is the overall goal of this thesis. The development of a device that meets these requirements is critical to transition the current practice of SHM to field deployment. The device that was designed was named the Wireless Impedance Device or WID.

The initial phase of the development [27, 7] was all done on prototype hardware, usually in the form of evaluation boards. The boards are large and require considerable power, but are easy to configure, allowing for changes to the overall setup to be made relatively quickly and easily. However, to make a device be used in real world situations requires the migration away from evaluation boards to a custom PCB (printed circuit board) configuration. The switch from pre-manufactured evaluation boards to a custom PCB required considerably more development for some of the components.

This chapter describes each component selection of the WID, the additional work required

to integrate those components onto a single board, and the results and comparison measurements from the final product. Much of the hardware investigation and proof of concept for the components used in the evaluation boards was performed in previous research.

In the development of the WID for structural health monitoring, three main areas were examined: The type of measurement to be made, the method of data transmission, and the method of power storage and delivery. In addition to these issues, as with any sensor node, certain consideration has to be paid to the type and complexity of the onboard data processing.

5.1.1 Impedance Method

Chapter 1 describes the impedance method in detail. However, two of the most important aspects of the impedance method are its lower power requirements than other active sensing methods and its ability to perform in-situ sensor diagnostics as discussed in Chapter 4. The low-cost and efficient capability of making real-world impedance measurement on field deployable SHM nodes has been made possible by a relatively new advance in integrated circuit impedance measurement technology at Analog Devices. The chips, which allow for the construction of the WID, are the AD5933 and AD5934. The AD5933 is of particular interest because of its higher capabilities. The AD5933 is equipped with a 12-bit 1MSPS A/D, a 1-100 kHz frequency range, and FFT functionality at the size of a small coin. These characteristics all lend this device to be used to create a self-contained, miniaturized, impedance-based structural health monitoring system.

5.1.2 Data Transmission

Wireless data transmission has two very desirable characteristics. Firstly, it eliminates the need for the installation and maintenance of the transmission wires. The wire installation has been demonstrated to be a significant part of the total system cost [37]. The lack of wires would also

eliminate a possible location for costly failures. Secondly, aside from the cost savings, it allows for the placement of sensor nodes in locations that could not accommodate a wired system, for example, on a piece of rotating machinery or structures in remote locations.

There have been several efforts in recent years to reduce the size and power requirements for several SHM systems. Tanner et al. [38] and Lynch et al. [39] examined wireless systems that measure analog sensors (i.e. accelerometers) and Grisso [26] has looked into wireless impedance measurements but with a significantly different component list than the one examined here. An overview of current wireless sensors systems is presented by Lynch and Loh [25].

5.1.3 Energy Harvesting and Delivery

The ability to have an efficient and inexpensive method to power wireless devices is an area of considerable research. Roundy et al. [40] gives an overview of potential power densities for different types of energy harvesting mediums, shown in Table 5.1.

Type	Power Density ($\mu W/cm^3$)
Solar - Outdoors	150-15000
Solar - Indoors	6
Piezoelectric Vibrations	250
Battery - Lithium	3.5
Battery - Lithium Rechargeable	0

Table 5.1: Power densities on a 10 year life span [40]

These various types of power might be used depending on the situation in which the sensor node resides. Because of the varying sources, the ability to accept a variety of power sources with little or no change to the device was also a priority. This feature would allow the device to be powered by a broad range of sources with minimal setup time. To accomplish this task, a charging circuit was introduced into the design. A simple circuit was designed utilizing a transistor that cuts power to the measurement circuit when voltage is applied at its

gate. Cutting power to the majority of the sensor node during the charging period allows for the power storage device to be charged more quickly. Conversely, the transistor will allow current to flow into the measurement circuit from the power storage, when the gate voltage is removed. The charging circuit would allow for various power sources to be easily used with minimal modification.

One method of energy delivery that is not examined in Table 5.1 is radio-frequency (RF) power transmission, and was one power source that was specifically taken into consideration with the design of the WID. In wireless power transmission, power is generated elsewhere and transmitted to a receiving system by some form of wave or radiation. The technology that has received the most attention in the last fifty years is that of microwave transmission. A pair of excellent survey articles were written to discuss the history of microwave power by Brown [41] and Maryniak [42]. Mascareñas [27] performed a preliminary study to show the feasibility of wireless power transmission to power a telemetry device. In that study, Mascareñas was able to power the wireless telemetry system and send several bytes of data, but the overall efficiency of the system was quite low. It is believed that significant improvements can be made to the system, so it is being studied further [7, 43].

5.1.4 Computational Requirements

The final requirement that must be addressed in any sensor node is the amount of on site processing power required. There is always a trade off between processing ability and power consumption. This trade off is not of concern with devices with a readily available power supply, but it is of utmost concern with wireless devices. Because of the lack of excess power in WID, a DSP (Digital Signal Processor) was not used because of its high energy requirements. In addition, its computational power was not vitally needed because much of the processing is done on the AD5933, with its built in FFT function.

Figure 5.1: Relative size of the AD5934, a sister chip to the AD5933 with a lower sampling rate

For the wireless impedance device, a processor has been chosen with the basic feature set to allow for impedance measurements to be made. These features include data reduction and external device control. The ability to expand for future applications through the use of an open development platform was also a consideration.

5.2 Hardware Selections and Considerations

5.2.1 AD5933

The main impedance component in the WID is the AD5933 chip from Analog Devices (AD) that allows for very low power high frequency impedance measurements to be taken. A picture of the AD5934, which is identical in size to the AD5933, is shown in Figure 5.1.

The method which the AD5933 uses to measure the impedance of a piezoelectric patch (PZT), is similar to the technique discussed by Peairs [44]. A diagram of the impedance circuit used in the AD5933 is shown in Figure 5.2.

The chip can be programmed to take an impedance measurement from 1-100 kHz, with a variety of voltage levels and input gains to make best use of the ADC. The AD5933/34 can take

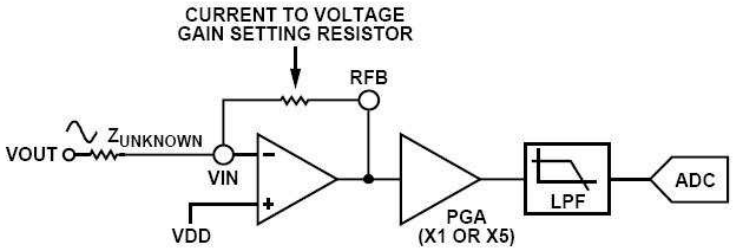

Figure 5.2: Impedance circuit used in the AD5933

as many as 512 points in a frequency sweep, for each point there will be an output stored in the output registers. The two registers are named *Real* (G_{reg}) and *Imaginary* ((B_{reg}) [45]. These names are unfortunate terminology, because the data that is in those registers does not directly represent real or imaginary numbers. The two registers represent the change in magnitude (Z) and phase (θ) of the impedance measurement, which are sufficient to obtain a very good measurement if a proper baseline is taken with a known impedance value i.e. a simple resister.

The AD5933 has been used in the past [27], but several important aspects of the impedance measurement were difficult to obtain. The most significant of these problems was the inability to separate a magnitude measurement into its corresponding real and imaginary components, which is necessary for SHM measurements. Through close work with Analog Devices, a procedure to obtain and accurate impedance measurement using the AD5933 was established.

Basic Measurement Procedure

There are several aspects of the measurement process with this chip that take special care to insure an accurate measurement.

1. The RFB resistor (Figure 5.2) should be chosen to be approximately equal to the midpoint impedance magnitude that will be observed in the frequency range of interest. This selection keeps the ADC from overloading or cropping the data.

2. The *Real* and *Imaginary* registers are used to calculate magnitude of the registers (Y_{reg}) as well as the phase of the registers (θ_{reg}) by the typical magnitude and phase calculations given in Equations 5.1 and 5.2. If a measurement is taken of a known resistance that has a zero phase component, then the phase that is calculated is the system phase (θ_{sys}), it is the offset from zero that is inherent to the chip. The system phase is a baseline, used to obtain the correct phase for future measurements. Y_{reg} and θ_{reg} are not to be confused with Z_{imp} and θ_{imp}, which are the final and accurate values for the impedance magnitude and phase after calibration.

$$Y_{reg} = \sqrt{G_{reg}^2 + B_{reg}^2} \tag{5.1}$$

$$\theta_{reg} = \arctan(\frac{B_{reg}}{G_{reg}}) \tag{5.2}$$

   (a) A possible consideration is the R_{out} of the chip. R_{out} is the DC impedance value of the chip itself, and depending on the measurement requirements, it may need to be calculated at least once. Each AD5933 has a unique DC impedance value associated with it. Various nominal values are given in the data sheet [45], but the value can vary substantially depending on the specific lot the chip came from. If the nominal value given in the data sheet will create a significant error in the measurement, R_{out} should be calculated. The easiest way to calculate this value is to take two impedance measurements with known resistances R_1 and R_2 and then back out the unknown R_{out}. The formula for R_{out} is given in Equation 5.3.

$$R_{out} = \frac{Y_{reg1} * R_1 - Y_{reg2} * R_2}{Y_{reg2} - Y_{reg1}} \tag{5.3}$$

3. Using Y_{reg}, the Gain Factor (GF) should be calculated according to Equation 5.4 using a

known calibration resistance R_{cal}. If the R_{out} is not needed, then use the same formula, but with $R_{out} = 0$

$$GF = \frac{\frac{1}{R_{cal}+R_{out}}}{Y_{reg}} \tag{5.4}$$

4. Once the GF and system phase are obtained, a measurement on an unknown test article can be made and the actual magnitude and phase of the test article can be calculated by using Equations 5.5 and 5.6.

$$Z_{imp} = \frac{1}{GF * Y_{reg}} \tag{5.5}$$

$$\theta_{imp} = \theta_{reg} - \theta_{sys} \tag{5.6}$$

Special Considerations for SHM

The above calculations, with step 2.a, will remove the R_{out} for a purely resistive or capacitive measurement. Calculations could be performed to remove the complex influence of a PZT transducer but it would require significant calibration measurements. These calibration measurements would be required each time if the impedance range, the RFB resistor, the excitation voltage, or the internal gain was changed.

Through interaction with Analog Devices, a method for removing the R_{out} has also been developed. This removal involves the use of an operational amplifier, or Op-Amp. When an Op-Amp is set up in a voltage follower (buffer) configuration, it has the effect of reducing the input impedance to near zero on the output. A circuit diagram of this setup can be found in Figure 5.3. This solution was not developed until after the first WID was constructed, so an Op-Amp is not integrated into the design.

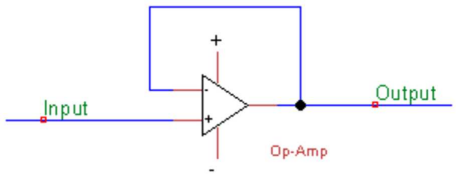

Figure 5.3: Operational amplifier set to voltage follower mode

When placed on the V_{out} line of the AD5933, the Op-Amp has the effect of virtually removing the DC impedance of the chip. This reduction is extremely useful because it eliminates the need for the additional calibration measurements, so only the GF calculation is necessary.

5.2.2 Power Storage

A goal for this device is to be able to power it up from an array of potential sources, and have it perform in-situ measurement and transmit the data to an accessible base station. In order to make these functions possible, an Areogel Supercapacitor from Cooper Bussmann has been included in the design, and would allow the device to store a lower current power source over a longer period of time to achieve an operable level of power to perform various test measurements. Also included in the design for power storage is the circuit to automatically cut power from the device when power is being received and to power on the device once the supercapacitor has reached its required charge, as well as a supercapacitor bypass jumper.

5.2.3 XBee RF Module

The telemetry system that is used on the WID is the XBee RF Module from MaxStream. The main advantage of the module is the low pin count required for operation. Aside from power and ground, it requires only two additional pins to enable it to act in serial line replacement mode (where it sends on everything it receives) [46]. In addition to those pins, the sleep pin

has also been routed to allow for lower power consumption.

Although the XBee is not the most power efficient telemetry solution on the market, as the transmission current is given as 45mA at 3.3V, it is perhaps one of the easiest to implement. For the initial development of the device, a simple and straight forward development process was weighed against total power consumption. In future versions of the impedance sensor node, a more power-efficient wireless-telemetry solution will be examined.

5.2.4 ATmega128L

The microprocessor that is being used is the ATmega128L from the Atmel corporation. The ATmega128L is the onboard computational core. It allows for onboard data processing and algorithm implementation. This microprocessor was chosen because it requires a low voltage (3V), has the proper interface (i^2c) to control the AD5933 and has the capability to be significantly expanded for future applications. This expansion includes added memory, added flash and control of additional components.

The ATmega128L comes from a line of microprocessors with support from a large open source development community. Atmel continues to develop new versions of the ATmega128 product line with enhanced capabilities. These capabilities include lower power consumption, more memory and more EEPROM. Atmel is adding these features while maintaining the same form factor, which allows for pin compatibility and makes easy upgrades of future versions of the WID possible.

5.3 Hardware Integration

The components discussed in Section 5.2 have been integrated into a complete device, the WID. The circuit diagram for this device is show in Figure 5.4. The circuit diagram shows the charging circuit as well as all the components and wiring paths. To produce the WID, the

schematic was taken from the diagram shown in Figure 5.4 and imported into a PCB (printed circuit board) program where it was prepared for manufacture.

The WID, as discussed, has the AD5933, ATmega128, XBee, and Supercapacitor components on the board. In addition to these components, it includes a crystal oscillator, battery hookup, various indicator LEDs, In System Programming (ISP) header, and voltage regulator. A 2.5mm phono jack was used to hook to the PZT patch being measured, which allowed for quick change between various PZT patches. A picture of the final WID is shown in Figure 5.5

5.4 Experimental Setup and Results

Experimental investigation was performed in order to confirm that the WID was capable of making all the necessary measurements used in impedance-based SHM, and to see if the power consumption was low enough to make it a practical wireless sensor node. For all of the testing performed, the WID was connected to a power supply though its power port and was programmed with the required frequency ranges and data acquisition points. Once the measurement was performed, the data was sent wirelessly to an XBee modem that was used as a serial port interface. Several MATLAB scripts were written to import the data from the serial port and perform basic calculations and plot the data.

Three different parts of an impedance measurement were recorded: real impedance, imaginary admittance and impedance magnitude. The real impedance is used in impedance-based SHM as the primary damage detection measurement, because it is more sensitive to damage or changes in the structure [9, 14]. The imaginary admittance measurement is used for sensor diagnostics, because the slope of the imaginary admittance line varies with PZT sensor condition [10, 6], which would include sensor debonding and sensor breakage. Finally, an impedance magnitude measurement was taken to examine the overall accuracy of the system, and to investigate possible procedures to improve the measurement in the future.

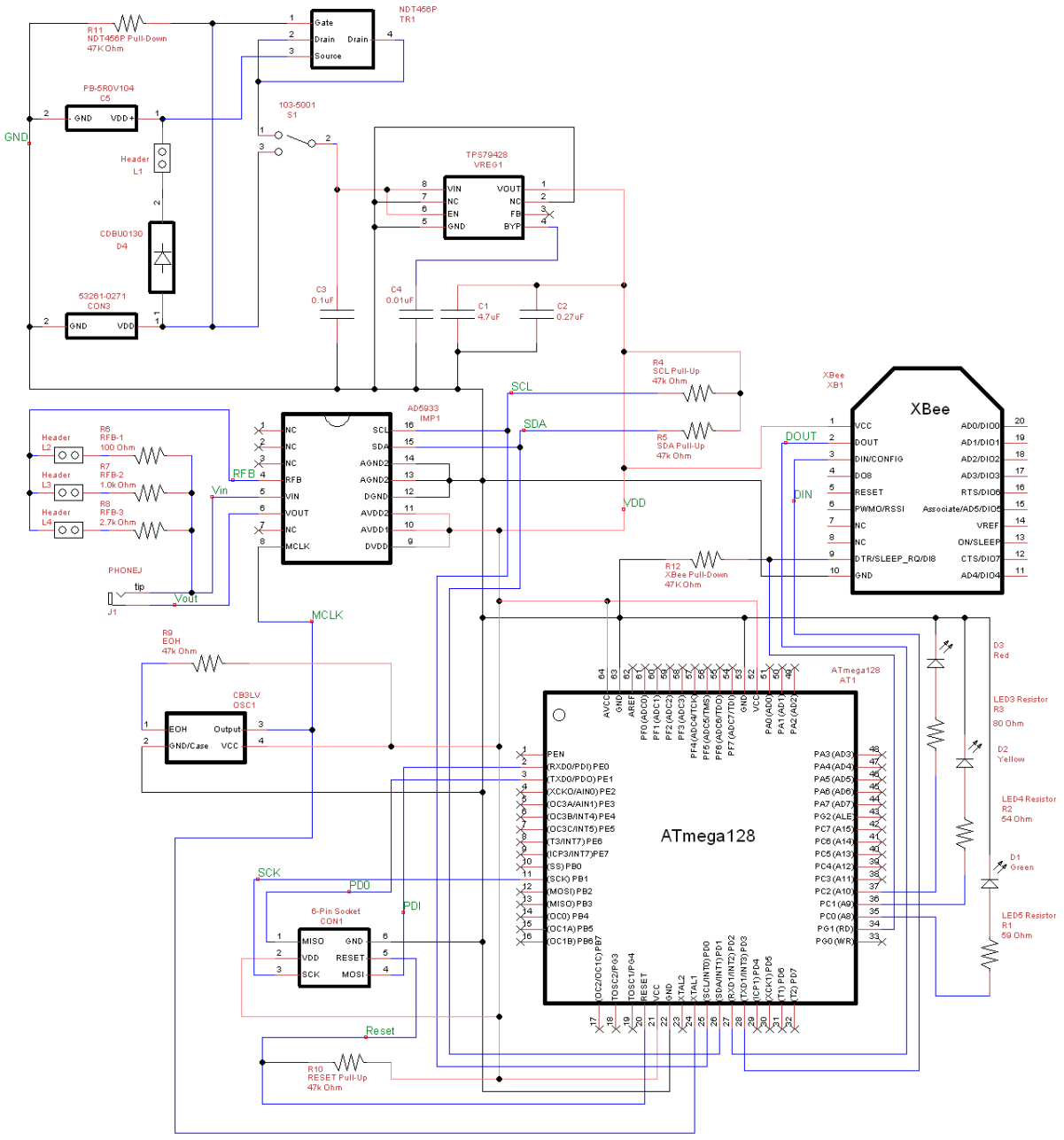

Figure 5.4: Circuit schematic of the WID

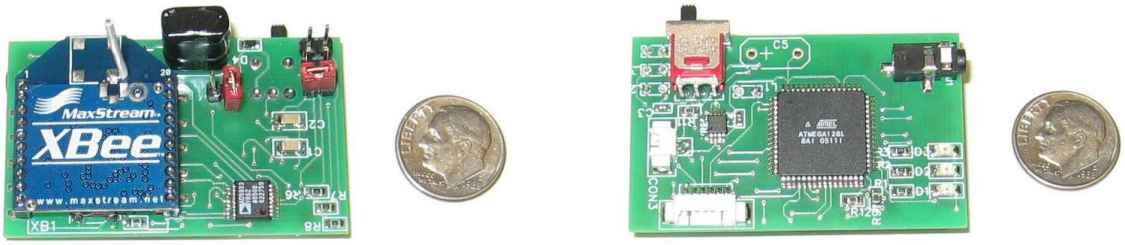

(a) Top (b) Bottom

Figure 5.5: Both sides of the Wireless Impedance Device

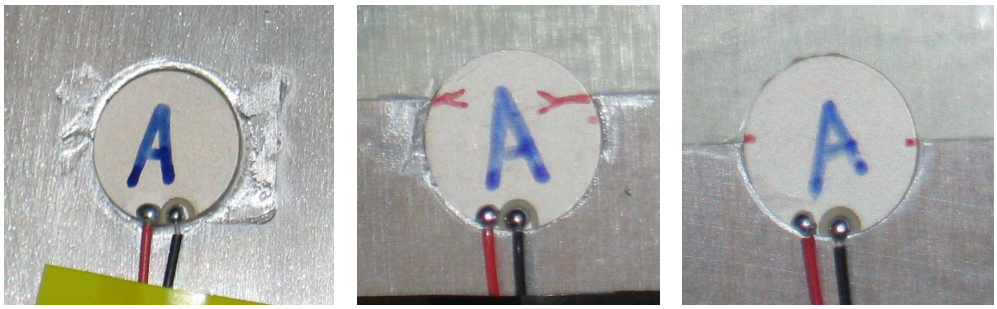

(a) 0% Debonding (b) 25% Debonding (c) 50% Debonding

Figure 5.6: Various debonding percentages on 12.7mm PZT patches

The piezoelectric patches that were measured were 12.7mm in diameter, 0.2mm thick and were bonded to a 6.35mm thick aluminum plate. For purposes of testing the imaginary admittance slope change, corresponding to bonding condition, three patches were bonded at all three debonding percentages: 0%, 25% and 50%. Achieving the specific debonding percentages was accomplished by bonding the patches on top of a corresponding percentage of double layer release paper. An example of the bonding conditions is shown in Figure 5.6.

In order to produce the most versatile device, consideration was given to making the WID have a small power requirement, which was achieved through the selection of parts discussed in Section 5.2. To determine the actual in-service power consumption, several tests were performed on the WID during various operational conditions to identify the useful life of the device with different power sources.

The power consumption measurements were taken during the previous measurements used to evaluate the impedance measurement capabilities of the WID. The addition of a multimeter allowed for the measurement of the current draw. The multimeter was placed in line on the WID's positive voltage terminal. A time reading was also taken to determine the length of each measurement phase.

5.4.1 Measurement Capabilities

To assess the capabilities of the WID, a comparison between the WID and an Agilent 4294A impedance analyzer was done. The testing was done to verify that any test or damage detection method that had been developed using a stand alone impedance analyzer could be performed using the WID. A variety of bonding conditions and excitation frequencies were examined.

Imaginary Admittance Measurement Comparison

The first comparison that was performed was to see if the WID was comparable to the Agilent in its ability to measure the imaginary impedance and relative changes in that measurement. The imaginary admittance measurements are shown in Figure 5.7.

The measurements from the WID are essentially the same as those from the Agilent impedance analyzer. As can be seen in the figure, the WID also captures the resonance changes in the different bonding conditions. There is a slight difference in the absolute value of the admittance from the WID to the Agilent; this change is due to the R_{out} of the AD5933, as described in the previous section. The relative changes are the same between the two devices, which indicates the WID can perform the necessary sensor diagnostics, for which this measurement is used.

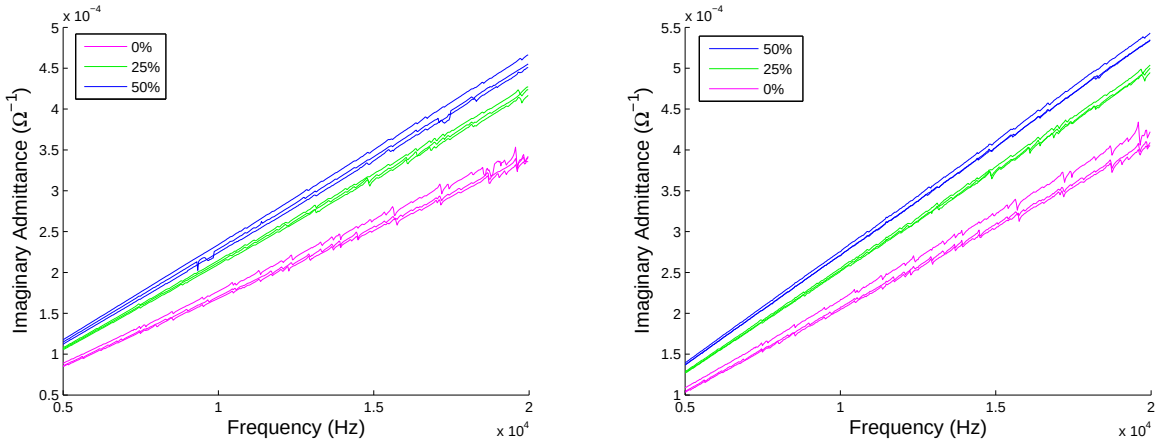

(a) Agilent (b) WID

Figure 5.7: Comparison of the imaginary admittance measurements of patches with various percentages of debonding.

Real Impedance Measurement Comparison

The second test determined see how well the WID measured the real impedance of a PZT patch. This measurement is the one used most often for damage detection in SHM. Two measurements, made several hours apart, were taken on both the Agilent impedance analyzer and the WID, which was done to compare the consistency of measurement in the devices, shown in Figure 5.8.

It can be seen in this graph that the WID captures all of the system dynamics. Its measurement and the measurement from the Agilent are of identical shapes, meaning the WID captures the system as well as the impedance analyzer. There is a difference in the magnitude because of the way that the phase was used to determine the real part of the measurement and from the contribution of R_{out}. These two factors combine to offset the value of the real impedance, and possibly reflect it about the x-axis if the offset takes the value negative. Because the absolute values of impedance are not of interest, just relative changes in the structure, this offset does not pose an issue for structural health monitoring.

A second important feature is the repeatability of the measurement made with a device.

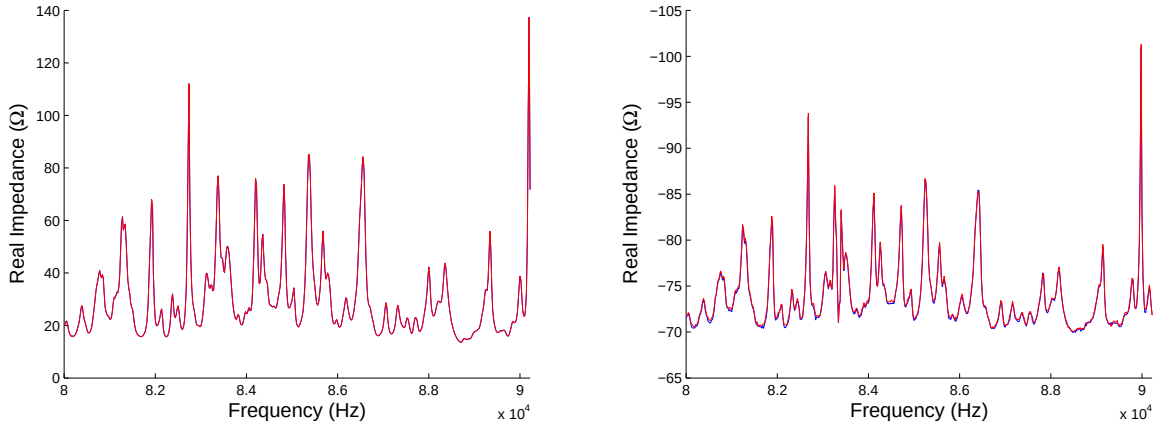

(a) Agilent (b) WID

Figure 5.8: Comparison of the real impedance measurements of the two devices on the frequency range of 80-90 kHz.

To test the repeatability of the two devices, two measurements were made with each and are displayed in Figures 5.8(a) and 5.8(b), they are both overlapping and virtually identical. All four measurements were taken on the same PZT patch, over the same frequency range, which allowed for the comparison of the signals. The two features of repeatability and overall shape accuracy allow the wireless impedance device to perform damage detection measurements.

Removing DC Impedance

To explore the influence of the Op-Amp solution (Section 5.2.1) on the impedance measurements of the WID, an Op-Amp was placed in line with the V_{out} pin of the AD5933. A magnitude measurement from 5-20 kHz was taken, and is shown in Figure 5.9.

Once the Op-Amp is in place, the WID gives a very accurate reading of impedance magnitude. The better match in measurement is the result of the reduction of the chips DC impedance value by the Op-Amp. The introduction of the Op-Amp did add noise to the measurement and distort the real part of the impedance. The cause of the noise is not known, and may be a product of the particular setup, and not an indication that all Op-Amps would affect the SHM

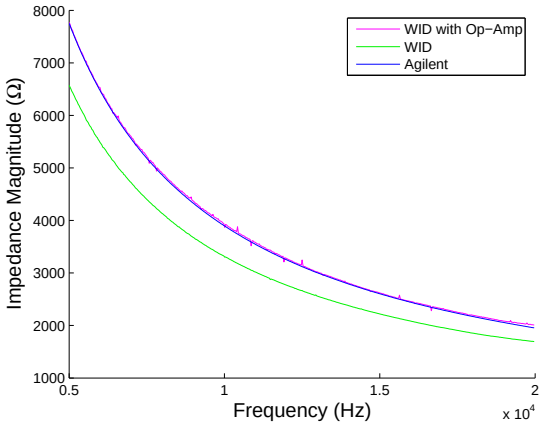

Figure 5.9: Impedance measurement of the WID with an Op-Amp buffer compared to the Agilent impedance analyzer and the WID without buffer on a frequency range of 5-20 kHz.

measurements in such a way. Regardless of whether the amplifier issues can be resolved, it has been shown that the WID, with an added Op-Amp, can make accurate magnitude measurements, and that the effects of the amplifier should be investigated further.

Comparison to the Agilent Impedance Analyzer

The WID is capable of making all the necessary SHM measurements and it requires significantly less power, is much more compact and costs a fraction of what the Agilent impedance analyzer does. The greater capabilities of the Agilent do not generally mean that it is more capable of making SHM measurements. For example, the WID does not have the total frequency range of the 4294A, which is probably the most significant disadvantage. However, impedance based structural health monitoring takes place well below 400 kHz [16], so most of the increased range of the 4294A is not used in the SHM field. Some of the important differences between the two devices are shown in Table 5.2.

The Agilent undoubtedly has an ADC with a higher bit count and sampling rate. However during testing of the WID, no problems have been encountered with the WID's 12-bit ADC

	4295A	WID
Frequency Range	40 Hz - 110 MHz	5 kHz -100 kHz
Sweep Points	801	512
Power Supply	120 V	2.8 V
Cost	$41,000	$200

Table 5.2: Comparison of key features between the Agilent 4294A and the WID

when the proper calibration procedure was followed. There is a limited amount of data storage and memory on the WID, which is currently the limiting factor for the processing capability of the device, but the Agilent has no ability to perform on board calculations. When the total cost of the two systems is taken into account, the WID is a considerable value.

5.4.2 Power Requirements

There are two main power consuming states that the WID could be in: measurement and transmission. A current reading was taken during both of these states to determine current draw. The results are shown in Table 5.3.

State	Current (mA)	Time (s)
Measure (XBee on)	68	16
Measure (XBee off)	17.5	16
Transmit	59.8	20

Table 5.3: Time and current draw to measure and transmit 512 data points of real and imaginary numbers

The results show very low power consumption, especially considering that no effort has been made for efficient measurement coding (i.e. sleep modes, data reduction prior to transmission and minimizing measurement points). It is thought that the power consumption could be further reduced if such changes were implemented.

To examine the potential of reducing the measurement power, a test was run with the XBee removed. According to the XBee data sheet [46], the sleep-state power consumption is $50\mu A$, which on a scale of mA is almost zero. It has a dramatic effect on the measurement

current draw level, bringing to it down to just under $18mA$. Considering the circuit is running at $2.8V$, the total power is just $50mW$. The current draw for the WID, with the XBee off, is also shown in Table 5.3.

5.5 Conclusions

The WID was developed to meet a need in the structural health monitoring field for a small, power efficient and flexible wireless impedance node. The size of the WID, at 5.2cm x 3.2cm, makes it a very portable and convenient device to use in various situations, especially compared to typical impedance analyzers with required power and data lines.

At the current levels of power consumption, the WID is at the lower extreme of the power consumption levels of devices presented in previous studies. The power levels observed are even more impressive when considering that this system performs active-sensing measurements, unlike most of the devices in those studies, which are passive measurement systems. At these power levels the WID could be powered by a wide range of energy harvesting methods. They would be at varying, but still reasonable duty cycle levels for SHM purposes.

There are several factors that contribute to the flexibility of the WID. First, the ability to quickly and efficiently change the code on the micro controller, through the onboard ISP header, allows one to perform a wide variety of data manipulation with minimal effort. Second, the ability to accept power from diverse sources through the built in power port and its low power consumption increase its versatility. Finally the inclusion of a wireless telemetry solution allows the sensor node to be placed in remote and inaccessible locations, without the constraints of a wire-based system. All of the above factors contribute to make the WID a very attractive device for the SHM community.

Future Work

A more versatile and power efficient model of the WID, the WID 2.0 is planned for the future, and should use many of the same components and algorithms. The WID 2.0 will take advantage of the recent power-efficient telemetry chips on the market, as well as multiplexing to have multi-sensor and auto-ranging capability. In addition, the use of the telemetry as an efficient trigger for the device is planned. The wireless trigger would allow for the device to be powered in virtually any manner, i.e. continuous or incremental power, and still be able to take measurements on demand.

Chapter 6

Integration of Software and Hardware Components for SHM

6.1 Introduction

The final stage in this thesis is to integrate the developed wireless impedance hardware and the sensor diagnostic algorithm with a suite of SHM software that was previously developed by Swartz et al. [36] in order to produce a complete solution for SHM application, which is the goal of this thesis. The program that will be modified for this integration is called HOPS, or Health of Plate Structures. This initial version contained geometry definition and lamb wave propagation analysis modules. Version two was subsequently developed by Jacobs et al. [47], and included impedance analysis and preliminary sensor diagnostics modules. HOPS has evolved from its initial design, and has started to become an integrated structural health monitoring application, with abilities to analyze both impedance and Lamb wave measurements. Two major components, which were missing from the HOPS program, were a robust sensor diagnostic algorithm and the ability to control external devices for the purposes of taking measurements. With the addition of these two abilities, and other general improvements, HOPS will have the ability to perform all the necessary tasks for a SHM application and will become a truly integrated SHM environment.

6.2 Main HOPS Interface and Improvements

The main interface of HOPS is the portal to which all of the SHM modules are accessed, and several general improvements were made to it for the sake of usability. The main window was changed to include more user feedback. Each module in HOPS passes its information to the next module when it is opened. However in the main HOPS window, there was no method for determining if there was data present, what the data contained, or what was the name of the file loaded. To resolve these issues several user feedback panels were added. A picture of the main HOPS window is shown in Figure 6.1.

Figure 6.1: The main HOPS module now gives important user feedback with regards to file information

In this figure, the main interface of HOPS can be seen. There are three main panels: *Setup, Current Data* and *SHM*. The *Setup* panel contains links to modules that let the user define geometry or import data from external sources. *Current Data* is a panel that allows for the manipulation of the currently loaded data. This manipulation of the data includes saving it

to a new file, clearing it for other modules or loading a previously recorded data set. The final panel, *SHM*, includes three links to modules that do the brunt of the SHM analysis. The three main capabilities include the analysis of Lamb wave propagations, the analysis of impedance based measurements and the diagnosis of sensor condition. If data is needed to be collected for these modules, that option is available from within the module itself.

There were also some other general improvements made in HOPS 3.0. The most important of these modifications is the new data storage method. The new method stores as many measurements as desired. This feature allows for the comparison of any two measurements in the file, HOPS 2.0 only stored the current and baseline measurements. The second major improvement was the modification of the geometry module, which facilitates the definition and importing of geometry files. This module was modified to accept the data from other modules; in preview versions, the data was erased whenever the geometry was defined. This improvement allows for geometry to be added at anytime in the measurement procedure, not just at the beginning. Finally, the impedance analysis module was modified to improve the user interface. During damage detection, certain damage indices are chosen and input by the user by examining additional figures and typing in appropriate values. In HOPS 3.0 the indices can be chosen directly in the GUI, simplifying the process and eliminating an area for potential errors. Other modifications include some general improvement of the GUI on most of the modules to have common locations for buttons, and more standardized layout from module to module. All of these modifications represent a significant improvement to HOPS even without considering the sensor diagnostic module and hardware control module.

6.3 Sensor Diagnostic Module in HOPS

From the main interface window, if the *Sensor Diagnostics* button is selected, the user has a choice of which of the three sensor diagnostic modules to use. The first two choices were

the original two rudimentary sensor diagnostics modules. The first module is used for sensor arrays and it simply displays the susceptance signals and the total areas under the line. These values are displayed to facilitate the user to determine which sensor(s) is unhealthy. There is no automatic recommendation to assist the user in determination of sensor health. The second interface is implemented for single sensor diagnostics using a baseline measurement. The user must compare the baseline and the current measurement and make a determination on whether the sensor is healthy. In this interface there is no ability to account for temperature. This interface will be removed or replaced in future versions of HOPS.

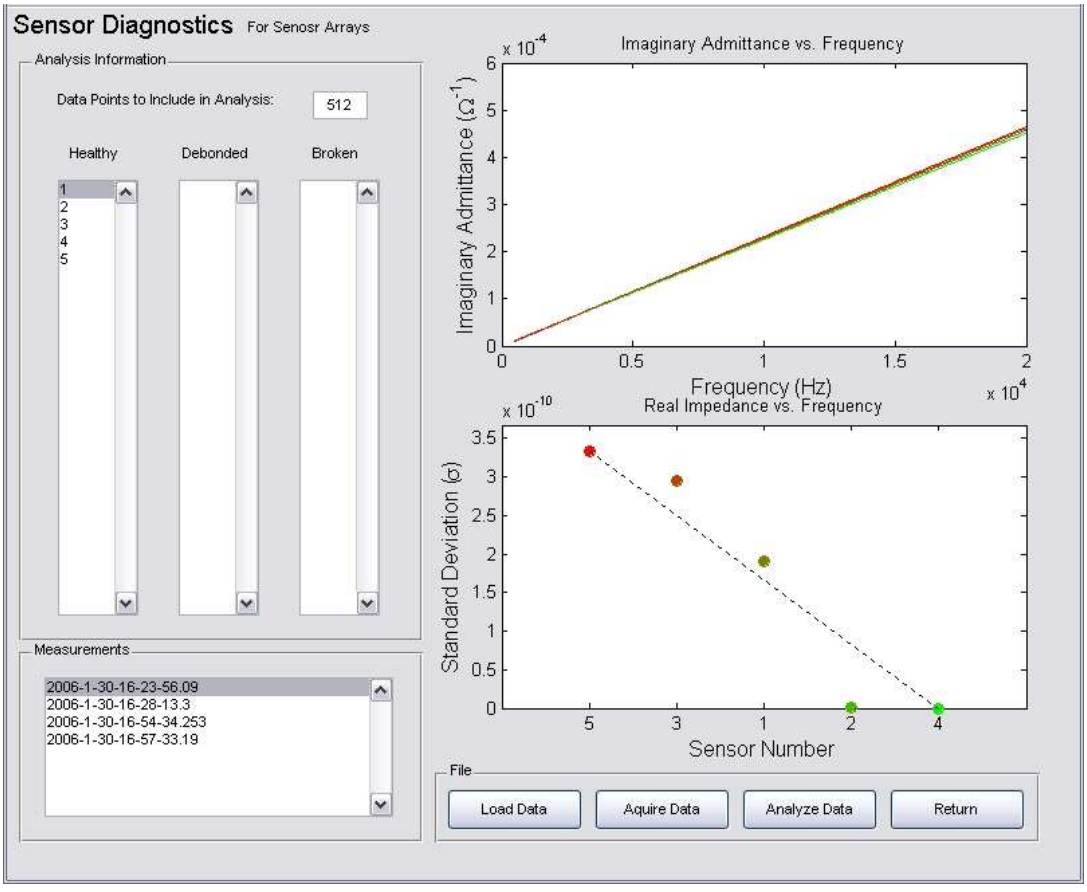

Figure 6.2: The sensor diagnostic module automatically determines which sensors are broken or debonded

The sensor diagnostic algorithm for sensor arrays that was developed in Chapter 4 was

implemented in the HOPS program as a third sensor diagnostic module. The GUI (graphical user interface) of the new module is shown in Figure 6.2. There are several key features to this interface. The first is the ability to select any of the past measurements in the file for analysis. The *Measurement* panel is where the measurement is selected and allows for comparison over time. The second important feature is the number of data points that to be included in the analysis can be selected. This selection is important to avoid possible structural resonances that could invalidate the algorithm. This parameter is set in the *Analysis Information* panel. Beyond these two user selectable parameters, the algorithm works as developed and described in Chapter 4

6.4 Structural Health Monitoring using External Devices

The final stage of integration performed on the HOPS software was the addition of a hardware control module. This control module was made to be available from both the impedance measurement and sensor diagnostic modules, which would allow for data to be acquired for both validation and SHM purposes. To date, in order to analyze data for sensor diagnostics or SHM purposes, impedance data had to be taken manually with an independent external impedance analyzer, formatted and imported into the HOPS program for analysis. The format of the information was not consistent and the process was time consuming. To alleviate this burden, the impedance data acquisition module was written and implemented. This module allows for the direct control of both the WID and an Agilent 4294A impedance analyzer. The acquisition module reduces the time required to measure multiple PZT transducers and eliminates the formatting issue associated with data coming from multiple sources. A picture of the acquisition module is shown in Figure 6.3.

The module has three main GUI panels: *Device, Measurements* and *Measurement Information*. The *Device* panel selects the device that will be used to take the measurement. The

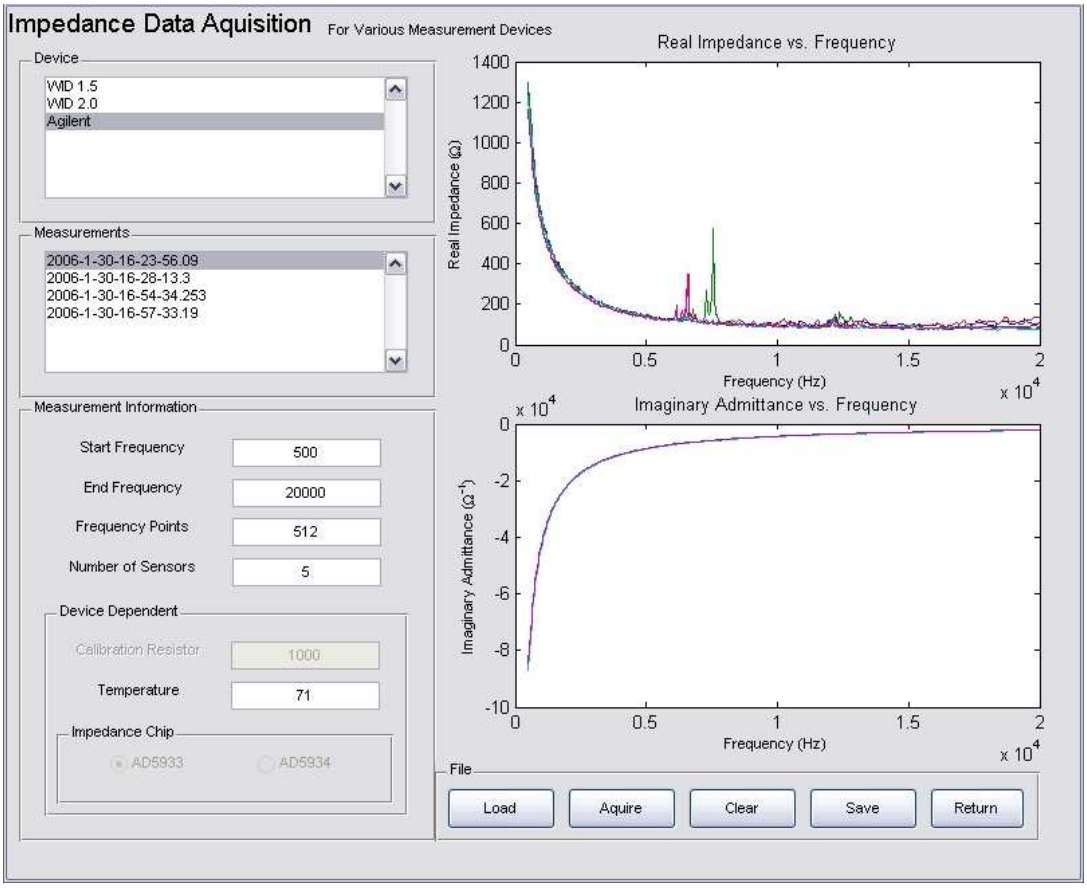

Figure 6.3: A module was added to allow for the control of external devices include the WID developed for this thesis

module currently has two devices implemented for control, the WID 1.5, which is the wireless device developed in this thesis, and an Agilent 4294A impedance analyzer. The *Measurements* panel shows the current measurements in the data file that is loaded. When the user selects past measurements, the graphical displays are updated to reflect the selection. The loaded file can also be cleared, if a new measurement file is desired. The final panel, *Measurement Information*, lets the user specify the several parameters that the measurement will have. These parameters include: start and stop frequencies, the number of data points, and the number of sensors in the array. In this panel there is also device dependent information. For example, the WID requires a calibration cycle, so the value for the calibration resistor can be input and the

Agilent can not take a temperature reading, so the value must be manually input.

6.5 Conclusions

Through the addition of the sensor diagnostic module and the added ability to control external impedance devices, this thesis work made HOPS into an integrated SHM application. This integration was the overall goal of this thesis. HOPS is capable of initiating a measurement, recording the results, validating the sensor array and analyzing for structural damage, all from its GUI. With the additional module for data acquisition, it will be possible to increase the number of devices that HOPS can control will minimal effort. Future iterations of the Wireless Impedance Device have already begun to be integrated with HOPS for increased functionality.

Chapter 7

Conclusions

7.1 Conclusions and Research Contributions

The need for an integrated SHM measurement system was primarily addressed in this thesis. A system that could measure, validate and analyze data in a single package did not exist for low-power SHM systems. This integration consists of three main components: construction of a low-power active-sensing field-deployable SHM node, development of a sensor-diagnostic algorithm for sensor arrays and the programming of an integrated SHM environment for hardware control and data analysis. The specific contributions of the three components are discussed further.

Impedance Hardware

The Wireless Impedance Device (WID) was developed to meet a need in the structural health monitoring field for a small, power efficient and flexible wireless impedance node. The size of the WID, at 5.2cm x 3.2cm, is a very portable and convenient device to use in various situations, especially compared to typical impedance analyzers with required power and data lines. The WID also moved beyond the currently available active measurement systems by being a stand-alone self-contained piece of hardware and not constructed of prototype hardware.

There are several factors that contribute to the flexibility of the Wireless Impedance Device. First, the ability to quickly and efficiently change the code on the micro controller, through the onboard ISP header, allows one to perform a wide variety of data manipulation with minimal effort. Second, the ability to accept power from diverse sources through the built in power port and its low power consumption allow the WID to be powered by a variety of methods. Finally, the inclusion of a wireless telemetry solution allows the sensor node to be placed in remote and inaccessible locations, without the constraints of a wire-based system.

At the current levels of power consumption, the WID is at the lower extreme of the power levels presented in previous studies. These power levels are low even though the WID is an active-sensing platform, unlike most of the devices in those studies, which dealt mostly with passive measurement systems. At these power levels the WID could be powered by a wide range of energy harvesting methods. All of the above characteristics make the WID the first deployable low-power impedance measurement node available for use.

Sensor Diagnostic Algorithm

The work done on the validation of sensor networks was the second major contribution of this thesis. The imaginary admittance method used in this algorithm showed its ability to validate a sensor system independent of temperature effects. The method can be readily used on sensor arrays with no pre-stored baseline measurements, and potentially on single sensors with baseline measurements. The method can also distinguish between sensor breakage and sensor debonding and give relative percentages of each, and is sensitive to small changes in either condition. The ability to determine the type of sensor failure had not been addressed in previous research. The affect of sensor failure on various SHM measurements was also quantified to allow for a more robust diagnostic procedure. In addition, impedance based measurement in the lower frequency ranges proposed here are more easily implemented with currently available hardware, and have lower power requirements than other methods.

Software Integration

The final contribution of this thesis is the combination of the hardware and software components into an integrated SHM system. This system, HOPS, combines the ability to measure data, validate the sensors, analyze the data for damage and display the results. Through the addition of the sensor diagnostic module and the added ability to control external impedance devices, HOPS has become a truly integrated SHM application. The final integrated solution was the culmination of this thesis, and no other similar system is known to exist. Future expandability of the system was also considered. It will be possible to increase the number of devices that HOPS can control with minimal effort, by simply adding modules for the specific hardware. Future iterations of the Wireless Impedance Device have already begun to be integrated with HOPS for increased functionality.

7.2 Future Work

The continued development of the WID for SHM purposes is a primary avenue for future work. It is believed that significant improvements can be made to the WID in future generations to include even lower power, greater versatility in energy delivery, increased number of sensors, and unique measurement triggering methods. Hardening the device for extreme environments is also considered an important direction of research, and will allow the WID to be deployed in extreme conditions.

The second main avenue for future work will be the integration of available hardware and software developments. This effort will continue to bring greater versatility to the integrated SHM system that was developed in this thesis. In addition, work on the single sensor validation procedure to include a robust regression technique, or the search for a temperature independent feature of the impedance measurement, should be considered. Although SHM systems gener-

ally have an array of sensors, any increase in versatility would be beneficial to the integrated environment.

Bibliography

[1] K. Worden and J. M. Dulieu-Barton. An overview of intelligent fault detection in systems and structures. *Structural Health Monitoring*, 3:85–98, March 2004.

[2] S. R. Hall. The effective management and use of structural health data. In Fu-Kuo Chang, editor, *Proceedings of the 2nd International Workshop on Structural Health Monitoring*, 1999.

[3] David W. Allen. Software for manipulating and embedding data interrogation algorithms into integrated systems. Master's thesis, Virginia Polytechnic Institute and State University, August 2004.

[4] Charles R. Farrar. An introduction to structural health monitoring. *Philosophical Transactions of The Royal Society*, 365:303–315, December 2006.

[5] C. Liang, F. P. Sun, and C. A. Rodgers. Coupled electromechanical analysis of adaptive material systems - determination of the actuator power consumption and system energy transfer. *Journal of Intelligent Material Systems and Structures*, 5:12–20, 1994.

[6] Gyuhae Park, Charles R. Farrar, Amanda C. Rutherford, and Amy N. Robertson. Piezoelectric active sensor self-diagnostics using electrical admittance measurements. *ASME Journal of Vibration and Acoustics*, 128(4):469–476, August 2006.

[7] Gyuhae Park, Timothy G. Overly, Matthew J. Nothnagel, Charles R. Farrar, David M. Mascareas, and Michael D. Todd. A wireless active-sensor node for impedance-based structural health monitoring. In *Proceedings of US-Korea Smart Structures Technology for Steel Structures,*, November 2006.

[8] Gyuhae Park, H. Sohn, Charles R. Farrar, and D. J. Inman. Overview of piezoelectric impedance-based health monitoring and path forward. *The Shock and Vibration Digest*, 35:451–463, 2003.

[9] Suresh Bhalla, Akshay S. K. Naidu, Chin W. Ong, and Chee-Kiong Soh. Practical issues in the implementation of electro-mechanical impedance technique for nde. In Erol C. Harvey, Derek Abbott, and Vijay K. Varadan, editors, *Proceedings of SPIE*, volume 4935, pages 484–494, November 2002.

[10] Suresh Bhalla and Chee Kiong Soh. Electromechanical impedance modeling for adhesively bonded piezo-transducers. *Journal of Intelligent Material Systems and Structures*, 15:955–972, December 2004.

[11] Victor Giurgiutiu and Andrei Zagrai. Damage detection in thin plates and aerospace structures with the electro-mechanical impedance method. *Structural Health Monitoring*, 4:99–118, 2005.

[12] Victor Giurgiutiu, Andrei Zagrai, and Jing Jing Bao. Damage identification in aging aircraft structures with piezoelectric wafer active sensors. *Journal of Intelligent Material Systems and Structures*, 15:673–687, September/October 2004.

[13] Victor Giurgiutiu and Andrei N. Zagrai. Embedded self-sensing piezoelectric active sensors for on-line structural identification. *Transactions of the ASME*, 124:116–125, January 2002.

[14] F. P. Sun, Z. Chaudhry, C. Liang, and C. A. Rogers. Truss structure integrity identification using pzt sensor-actuator. *Journal of Intelligent Material Systems and Structures*, 6:134–139, January 1995.

[15] J. P Stokes and G. L. Cloud. The application of interferometric techniques to the nondestructive inspection of fiber-reinforced materials. *Experimental Mechanics*, 33:314–319, 1993.

[16] J. Esteban. *Modeling of the Sensing Region of a Piezoelectric Actuator/Sensor*. PhD thesis, Virginia Polytechnic Institute and State University, Blacksburg, VA, 1996.

[17] Gyuhae Park, Charles R. Farrar, Francesco Lanza di Scalea, and Stefano Corria. Performance assessment and validation of piezoelectric active-sensors in structural health monitoring. *Smart Materials and Structures*, 15(6):1673–1683, December 2006.

[18] Karl F. Graff. *Wave Motion in Elastic Solids*. Ohio State University Press, 1975.

[19] Horace Lamb. On waves in an elastic plate. In *Proceedings of the Royal Society of London*, 1917.

[20] Joseph L. Rose. *Ultrasonic Waves in Solid Media*. Cambridge University Press, 2000.

[21] D. C. Worlton. Ultrasonic testing with lamb waves. *Non-Destructive Testing*, 15:218–222, 1957.

[22] R. P. Dalton, P. Cawley, and M. J. S. Lowe. The potential of guided waves for monitoring large areas of metallic aircraft fuselage structure. *Journal of Nondestructive Evaluation*, 20(1):29–45, 2001.

[23] M. J. S. Lowe, D. N. Alleyne, and P. Cawley. Defect detection in pipes using guided waves. *Ultrasonics*, 36:147–154, 1998.

[24] Peter Cawley and David Alleyne. The use of lamb waves for the long range inspection of large structures. *Ultrasonics*, 34:287–290, 1996.

[25] Jerome P. Lynch and Kennith J. Loh. A summary review of wireless sensors and sensor networks for structural health monitoring. *The Shock and Vibration Digest*, 38(2):91–128, March 2006.

[26] Benjamin L. Grisso. Considerations of the impedance method, wave propagation, and wireless systems for structural health monitoring. Master's thesis, Virginia Polytechnic Institute and State University, 2004.

[27] David Dennis Lee Mascareñas. Development of and impedance method-based wireless sensor node for monitoring of bolted joint preload. Master's thesis, University of California, San Diego, 2006.

[28] M. I. Friswell and D. J. Inman. Sensor validation for smart structures. *Journal of Intelligent Material Systems and Structures Online*, 10:973–982, 1999.

[29] Maher Abdelghani and Michael I. Friswell. Sensor validation for structural systems with multiplicative sensor faults. *Mechanical Systems and Signal Processing*, 21:270–279, 2007.

[30] K. Worden. Sensor validation and correction using auto-associative neural networks and principal component analysis. In *Proceedings of the IMAC-XXI*. SEM, 2003.

[31] N. Saint-Pierre, Y. Jayet, I. Perrissin-Fabert, and J. C. Baboux. The influence of bonding defects on the electric impedance of a piezoelectric embedded element. *Journal of Physics D: Applied Physics*, 29(12):2976–2982, December 1996.

[32] D. Pacou, M. Pernice, M. Dupont, and D. Osmont. Study of the interaction between bonded piezo-electric devices and plates. In *1st European Workshop on Structural Health Monitoring*, number 155, 2002.

[33] E. F. Crawley and J de Luis. Use of piezoelectric actuators as elements of intelligent structures. *AIAA Journal*, 25(10):1373–1385, 1987.

[34] Jayant Sirohi and Inderjit Chopra. Fundamental understanding of piezoelectric strain sensors. *Journal of Intellignet Material Systems and Structures*, 11:246–257, 2000.

[35] Christopher Park, Curtis Walz, and Inderjit Chopra. Bending and torsion models of beams with induced-strain actuators. *Smart Materials and Structures*, 5:98–113, 1996.

[36] R. Andrew Swartz, Eric Flynn, Daniel Backman, R. Jason Hundhausen, and Gyuhae Park. Active piezoelectric sensing for damage identification in honeycomb aluminum panels. In *Proceedings of the IMAC-XXIV*. SEM, 2006.

[37] Mehmet Çelebi. Seismic instrumentation of buildings (with emphasis on federal buildings). Project 0-7460-68170, USGS, 2002.

[38] Neal A. Tanner, Jeannette R. Wait, Charles R. Farrar, and Hoon Sohn. Structural health monitoring using modular wireless sensors. *Journal of Intelligent Material Systems and Structures*, 14:43–56, 2003.

[39] Jerome Peter Lynch, Arvind Sundararajan, Kincho H. Law, Anne S. Kiremidjian, and Ed Carryer. Embedding damage detection algorithms in a wireless sensing unit for operational power efficiency. *Smart Materials and Structures*, 13:800–810, 2004.

[40] Shad Roundy, Paul K. Wright, and Jan Rabaey. A study of low level vibrations as a power source for wireless sensor nodes. *Computer Communications*, 26(11):1131–1144, July 2003.

[41] W. C. Brown. The history of wireless power transmission. *Solar Energy*, 56(1):3–21, 1996.

[42] G. E. Maynaiak. Status of international ezperimentation in wireless power transmission. *Solar Energy*, 56(1):87–91, 1996.

[43] Mathew Nothnagel, Gyuhae Park, and Charles R. Farrar. Wireless energy transmission for embedded sensor nodes. In *Proceedings of SPIE*, volume 6530, 2007.

[44] Daniel M. Peairs, Gyuhae Park, and Daniel J. Inman. Improving accessibility of the impedance-based structural health monitoring method. *Journal of Intelligent Material Systems and Structures*, 15:129–139, 2004.

[45] Analog Devices, www.analog.com. *AD5933 Data Sheet: 1MSPS, 12-Bit Impedance Converter, Network Analyzer*, rev. 0 edition.

[46] MaxStream, www.MaxStream.net. *XBee/XBee-PRO OEM RF Modules Product Manual*, v1.x82 edition.

[47] Laura D Jacobs, Gyuhae Park, and Charles R. Farrar. Development of an integrated software solution for piezoelectric active-sensing in structural health monitoring. In *Proceedings of SPIE*, volume X, 2007.